HOWARD UNIVERSITY
SCHOOL OF ENGINEERING
DEPARTMENT OF MECHANICAL ENGINEERING
WASHINGTON, D.C. 20059

FINAL REPORT

NASA GRANT: NSG-1414, Suppl. 5

THE DYNAMICS AND CONTROL OF LARGE FLEXIBLE SPACE STRUCTURES - VI

by

Peter M. Bainum
Professor of Aerospace Engineering
Principal Investigator

and

A.S.S.R. Reddy
Assistant Professor

and

R. Krishna
Cheick M. Diarra
Greduate Research Assistants

SEPTEMBER 1983

HOWARD UNIVERSITY
SCHOOL OF ENGINEERING
DEPARTMENT OF MECHANICAL ENGINEERING
WASHINGTON, D.C. 20059

FINAL REPORT

NASA GRANT: NSG-1414, Suppl. 5

THE DYNAMICS AND CONTROL OF LARGE FLEXIBLE SPACE STRUCTURES-VI

by

Peter M. Bainum
Professor of Aerospace Engineering
Principal Investigator

and

A.S.S.R. Reddy
Assistant Professor

and

R. Krishna
Cheick M. Diarra
Graduate Research Assistants

September 1983

ABSTRACT

The controls analysis based on a truncated finite element model of the 122m. Hoop/Column Antenna System focuses on an analysis of the controllability as well as the synthesis of control laws. Graph theoretic techniques are employed to consider controllability for different combinations of number and locations of actuators. Control law synthesis is based on an application of the linear regulator theory as well as pole placement techniques. Placement of an actuator on the hoop can result in a noticeable improvement in the transient characteristics. The problem of orientation and shape control of an orbiting flexible beam, previously examined, is now extended to include the influence of solar radiation evironmental forces. For extremely flexible thin structures modification of control laws may be required and techniques for accomplishing this are explained. Effects of environmental torques are also included in previously developed models of orbiting flexible thin platforms, and a preliminary analysis of related thermally induced deflections and torques on thin structures is provided. Finally, it is concluded, based on an evaluation of the coupling coefficients in the rigid modal equations and the generic modal equations for the first seven modes of the Hoop/Column System, that when the system is performing within nominal specifications (surface deflections of the order of mm), that the relative magnitude of the largest of these coefficients is at least one order of magnitude smaller than the principal coefficients.

CONTENTS

LIST OF FIGURES

LIST OF FIGURES

LIST OF FIGURES

LIST OF FIGURES

I. INTRODUCTION

The present grant extends the research effort initiated in previous grant years (May 1977 - May 1982) and reported in Refs. 1-8*. Techniques for controlling both the shape and orientation of very large inherently flexible proposed future spacecraft systems are being studied. Possible applications of such large structures in orbit include: large scale multi-beam communications systems; earth observation and resource sensing systems;orbitally based electronic mail transmission; and as orbital platforms for the collection of solar energy and transmission (via microwave) to earth based receivers.

This report is subdivided into seven chapters. Chapter II is based primarily on a paper to be presented at the 34th International Astronautical Congress and presents preliminary results on the controllability and control law synthesis for the Hoop/Column orbiting large flexible antenna system. Graph theoretic techniques previously introduced in Ref. 7 and further described in Ref. 8 are employed to consider system controllability for different proposed actuator arrangements (number and location). Control laws are then designed based on the ORACLS computer algorithm[9], primarily using linear quadratic Gaussian techniques. The mode shapes (eigenvectors) and frequencies of the system were obtained previously by finite element techniques and supplied by NASA-LRC.[10]

At the operational altitudes of the future missions involving large space structures, the principal environmental disturbance is

*For references cited in this report, please see list of references at the end of each chapter.

that due to solar radiation pressure. The effect of solar radiation (pressure) disturbance on a flexible uncontrolled orbiting free-free beam was examined in Ref. 8, and to the authors' knowledge represented a first attempt to include such disturbances in the system dynamics of a flexible structure in orbit. Chapter III of this report, based on a paper recently presented at the 1983 AAS/AIAA Astrodynamics Conference, extends this work to consider the closed loop dynamics of an orbiting flexible beam under the influence of solar pressure induced moments. Actuator control laws previously designed for the case where environmental effects were neglected are now re-evaluated especially for extremely flexible beams. Shape and orientation control (about two different nominal orientations - local horizontal and local vertical) are considered.

In Chapter IV, the effect of solar radiation pressure on the open-loop dynamics of a more complex structure, a thin homogeneous flexible square plate is analyzed. The mode shapes and frequencies of the plate are obtained numerically using a finite element computer algorithm. As in the case of the beam only small transverse deformations are assumed.

Solar pressure torques can also result on large flexible space structures due to the interaction of the incident solar radiation on the thermally deflected bodies. Chapter V presents a preliminary formulation of the solar radiation heating effects on thin rectangular plates and beams. The amount of thermal deflection depends on the thermal gradient across the structure, the thermal conductivity of the material, the thermal expansion coefficient, and the thickness. Expressions for the thermal gradients can be obtained by simultaneously considering

the thermal radiation and heat conduction properties. These expressions can be used to develop equations for the thermal deflections and subsequently a model for the induced moments on the (thermally) deflected structure. These moments will have to be considered in addition to those generated by the interaction of solar pressure on the freely vibrating system.

Chapter VI describes the development of a computer algorithm to evaluate the relative magnitude of coupling coefficients in both the rigid and elastic modal equations of motion. These coefficients describe coupling between the rigid and flexible modes and also intramodal coupling and are usually neglected when a finite element analysis is employed. The evaluation of the relative magnitude of these coefficients is based on the numerical parameters for the Hoop/Column system.

Chapter VII describes the main general conclusions together with future recommendations. The effort described in Chapters II, IV, and V is being continued during the 1983-84 grant period in accordance with our proposal submitted Jan. 1983.[11]

References

1. Bainum, P.M. and Sellappan, R., "The Dynamics and Control of Large Flexible Space Structures," Final Report NASA Grant: NSG-1414, Part A: Discrete Model and Modal Control, Howard University, May 1978.

2. Bainum, Peter M., Kumar, V.K., and James, Paul K., "The Dynamics and Control of Large Flexible Space Structures," Final Report, NASA Grant: NSG-1414, Part B: Development of Continuum Model and Computer Simulation, Howard University, May 1978.

3. Bainum, P.M. and Reddy, A.S.S.R., "The Dynamics and Control of Large Flexible Space Structures II," Final Report, NASA Grant NSG-1414, Suppl. I, Part A: Shape and Orientation Control Using Point Actuators, Howard University, June 1979.

4. Bainum, P.M., James, P.K., Krishna, R., and Kumar, V.K., "The Dynamics and Control of Large Flexible Space Structures II" Final Report, NASA Grant NSG-1414, Suppl. 1, Part B: Model Development and Computer Simulation, Howard University, June 1979.

5. Bainum, P.M., Krishna, R., and James, P.K., "The Dynamics and Control of Large Flexible Space Structures III," Final Report, NASA Grant NSG-1414, Suppl. 2, Part A: Shape and Orientation Control of a Platform in Orbit Using Point Actuators, Howard University, June 1980.

6. Bainum, P.M. and Kumar, V.K., "The Dynamics and Control of Large Flexible Space Structures III," Final Report, NASA Grant NSG-1414, Suppl. 2, Part B: The Modelling, Dynamics and Stability of Large Earth Pointing Orbiting Structures, Howard University, September 1980.

7. Bainum, P.M., Kumar, V.K., Krishna, R. and Reddy, A.S.S.R., "The Dynamics and Control of Large Flexible Space Structures IV," Final Report, NASA Grant NSG-1414, Suppl. 3, NASA CR-165815, Howard University, August 1981.

8. Bainum, P.M., Reddy, A.S.S.R., Krishna, R., Diarra, C.M., and Kumar, V.K., "The Dynamics and Control of Large Flexible Space Structures V", Final Report, NASA Grant NSG-1414, Suppl. 4, NASA CR-169360, Howard University, August 1982.

9. Armstrong, E.S., "ORACLS - A System for Linear Quadratic-Gaussian Control Law Design," NASA Technical Paper 1106, April 1978.

10. "Versatile Hoop/Column Antenna Structural Dynamic Model," unpublished report, prepared by the Harris Corporation, 1982 (transmitted via NASA-LRC).

11. Bainum, P.M. and Reddy, A.S.S.R., "Proposal for Research Grant on: The Dynamics and Control of Large Flexible Space Structures VII," Howard University (submitted to NASA), Jan. 15, 1983.

II. ON THE CONTROLLABILITY AND CONTROL LAW DESIGN FOR AN ORBITING LARGE FLEXIBLE ANTENNA SYSTEM

Abstract

The controllability and control law synthesis based on a finite element model of the Hoop/Column orbiting antenna system is considered. Graph theoretic techniques are employed to analyze the controllability of the system for possible proposed actuator arrangements which include torquers and point actuators along the mast and a single actuator placed on the hoop assembly. Once controllability is established for a given combination of number and location of actuators, the synthesis of control laws is based on an application of the linear regulator theory and also pole placement techniques. In general, surface torsion and feed mast torsion are among modes having the longest time constants. System transient performance is noticeably degraded when the hoop actuator is not included.

I. Introduction

Large flexible orbiting systems have been proposed for possible use in communications, electronic orbital based mail systems, detection of earth resources, and in solar energy collection. The size and low weight to area ratio of such systems dictate that system flexibility is now the main consideration in the dynamics and control problem as contrasted with the inherently rigid nature of earlier spacecraft systems. For such large flexible systems both orientation and shape control will often be required. It is the purpose of the present paper to consider the controllability and the subsequent design of control laws based on a model of a proposed orbiting antenna system - the Hoop/Column system.

The Hoop/Column antenna system is one of the configurations under consideration for use in the future multi-beam Land Mobile Satellite System[1], designed to provide point to point communications for 250,000 subscribers across the U.S. in the mid 1990's. The system is based on a large geosynchronous relay antenna and a number of mobile, Earth-based receivers. In order to achieve the required RF performance a pointing accuracy of ± (0.03 - 0.10) degree RMS and a surface (antenna) accuracy of 12mm RMS will be required. The Hoop/Column antenna system[2], depicted in Fig. 1, in deployed configuration, contains the deployable (telescoping) mast system connected to the hoop by support cables under tension.

The hoop contains 48 rigid sections, to be deployed by motor drive units. The desired shape of the RF reflective mesh is produced by a secondary drawing surface using surface control cables. The reflective mesh is connected to the hoop by quartz or graphite stringers. At one end of the mast the electronic feed assemblies are positioned, whereas at the other end are the principal solar arrays connected to the main bus based control.

Recently graph theoretic techniques[3] were used to study controllability of linear systems which could represent large flexible orbiting systems with inherent damping. It was seen that the term rank deficiency in the stiffness matrix dictates the required number as well as the location of the actuators required for controllability, whereas the presence of the damping matrix does not influence the required number of actuators but provides greater flexibility to the available actuator locations for which the system is controllable. Specific examples were based on a previously developed model[4] of an assumed homogeneous shallow thin spherical shell in orbit, where both orientation and shape control were assumed to be provided by point actuators placed on the shell's surface.

It is the objective of this paper to apply these techniques, first to analyze the controllability of the Hoop/Column system based on a possible arrangement of actuators, and, once controllability is assured, to consider various ways to develop control laws. A recent related treatment[5] of the preliminary controls synthesis for this system was based on a model which contained three rigid-body rotational modes and a number of flexural modes, but ignored the three rigid translational modes. Actuators in the form of torquers only, were assumed to be placed only along the mast assembly, and controllability was established indirectly through numerical means. Control synthesis was accomplished based on linear quadratic Caussian techniques and also a related linear analysis assuming the collocation of actuators and sensors.

II. Mathematical Model

In the present paper, a finite element model of the Hoop/Column system that includes all six rigid modes and the flexural modes is used. For the purposes of this study the system is modelled using 112 node (grid points) with each node having a maximum of six degrees of freedom.[6] Thus, the linearized dynamics of the Hoop/Column antenna system can be described (in the absence of structural or other damping) by:

$$M\ddot{X} + KX = F_c \qquad (1)$$

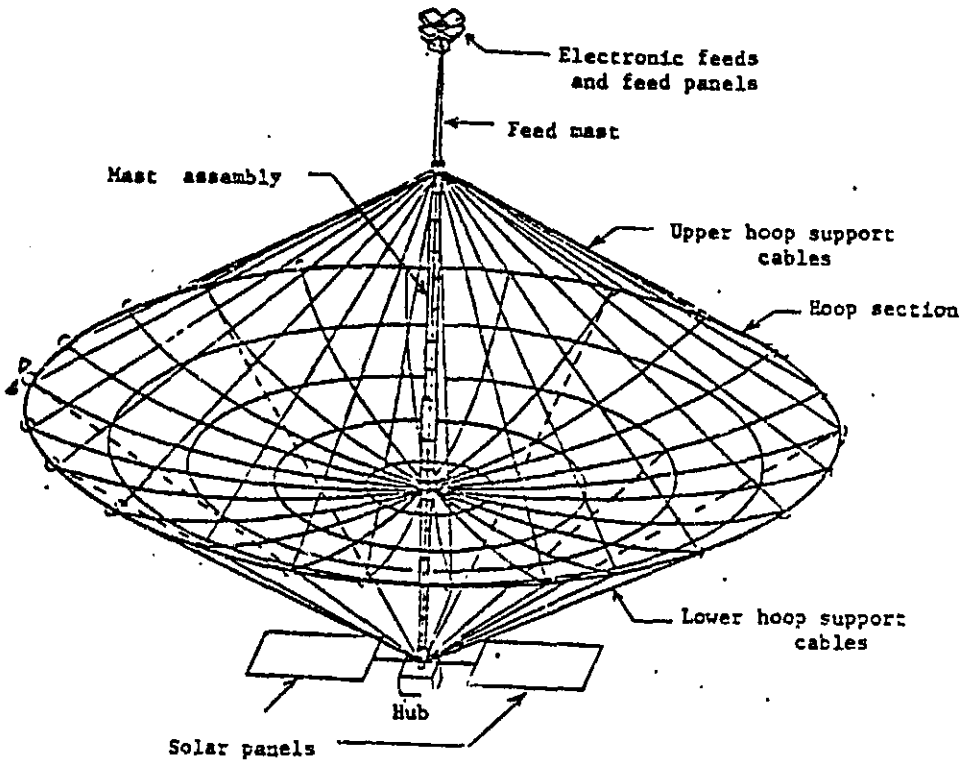

Fig. 1. The Hoop/Column antenna system.

where

M is the 672x672 mass/inertia matrix
K is the 672x672 stiffness matrix
X is the 672x1 matrix consisting of the displacements and rotations at the nodal points
F_c is the control vector of dimensionality 672x1

After using the transformation between the modal coordinates, q, and X given by

$$X = \phi q \tag{2}$$

equation (1) can be rewritten as:

$$\phi^T M \phi \ddot{q} + \phi^T K \phi q = \phi^T F_c \tag{3}$$

The left side of equation (3) can be expressed in terms of diagonal matrices, based on the properties of the eigenvalues and associated eigenvectors, according to:

$$[\tilde{m}_i]\ddot{q} + [\tilde{K}_i]\, q = \phi^T F_c \tag{4}$$

where

$\phi^T M \phi$ = diag. $[m_i] = [\tilde{m}_i]$
$\phi^T K \phi$ = diag. $[K_i] = [\tilde{K}_i]$
m_i = i^{th} generalized (modal) mass
K_i = i^{th} generalized stiffness.

The first thirty-four (including the six rigid modes) eigenvectors and eigenvalues derived from the NASTRAN software for the system described by equations (1) and (2) were supplied; however, only the first 26 modes had appreciable non-zero values for the corresponding modal masses.

The influence of a finite number (m) of control actuators or torquers is incorporated into the model by

$$F_c = BU \tag{5}$$

where

B = 672xm control influence matrix
U = mx1 matrix associated with the control vector

The control influence matrix, B, (672xm) is formed as follows:

If there is an actuator that influences the i^{th} node ($1 \leq i < 112$) in the j^{th} direction ($1 \leq j \leq 6$), then B(K,L)=1 where K = (i-1)x6+j, and L = number of the actuator. Thus the B matrix consists of zeros and ones, showing the influence of the force actuators on the translational degrees of freedom of the nodes, and also that of the torque actuators on the rotational degrees of freedom.

The model considered here consists of six rigid body modes (3 translation + 3 rotation) and the first seven flexible modes. The values of the generalized masses and stiffnesses are listed in Table 1.

Table 1 - Hoop/Column single layer surface model eigenvalues

Mode No.	Frequency Hz	Generalized mass, m_i (lb-sec^2/in)	Generalized K_i Stiffness (lb/in)
1	0.0	16.44388	0.0
2	0.0	8.925020	0.0
3	0.0	7.349353	0.0
4	0.0	9.704152	0.0
5	0.0	2.940652	0.0
6	0.0	8.418909	0.0
7	.1188347	153.1373	85.38542
8	.2142455	2.232954	9.482657
9	.2709558	3.073094	8.907021
10	.5063228	.3046446	3.083247
11	.7288725	1.992988	40.88663
12	.8897594	723.5216	22612.90
13	.9192313	.6581203	21.95405

III. Controllability Considerations

Equation (4) can be rewritten with the aid of equation(5) as:

$$\ddot{q} = -[\tilde{m}_i]^{-1}[\tilde{K}_i]\, q + [\tilde{m}_i]^{-1}\phi^T B U \tag{6}$$

and then cast into standard state space format with the result:

$$\begin{bmatrix} \dot{q} \\ \ddot{q} \end{bmatrix} = \left[\begin{array}{c|c} 0 & I \\ \hline -[\tilde{m}_i]^{-1}[\tilde{K}_i] & 0 \end{array}\right] \begin{bmatrix} q \\ \dot{q} \end{bmatrix} + \begin{bmatrix} 0 \\ \hline [\tilde{m}_i]^{-1}\phi^T B \end{bmatrix} U \tag{7}$$

The number and location of the actuators are determined after considering the controllability in addition to physical considerations. The dynamic system represented by equation (7) is controllable[7] if and only if the pair

$-[\tilde{m}_i]^{-1}[\tilde{K}_i]$ and $[\tilde{m}_i]^{-1}\phi^T B$ is controllable.

The system matrix, $S = -[\tilde{m}_i]^{-1}[\tilde{K}_i]$ for the 13 mode model can be evaluated as:

$$S = \begin{bmatrix} 0 & 0 & 0 & 0 & 0 & 0 & & & & & & & \\ & & & & & & -K_7/m_7 & & & & & & \\ & & & & & & & \ddots & & & & & \\ & & & & & & & & \ddots & & & & \\ & & & & & & & & & \ddots & & & \\ & & & & & & & & & & -K_{13}/m_{13} & & \end{bmatrix} \tag{8}$$

The digraph of the matrix S is shown in Fig. 2. For controllability[3] the actuators must be placed in such a way that they will influence all the modes directly since, in this model, there is no coupling between the modes. The number of actuators will be dictated by the term rank (7) of the matrix, S. Because of the six rigid modes (with zero eigenvalues), the system matrix, S, has a rank deficiency of six; to augment the term rank $[\phi^T B]$ must have at least six linearly independent non-zero columns, indicating a minimum of six properly placed actuators is needed for controllability.

A possible proposed arrangement of a maximum of 13 actuators consisting of combinations of point actuators and a torquer, assumed to be located along the mast and at selected points in the feed assembly, is depicted in Fig. 3. In addition, a single point actuator is assumed to be positioned on one of the rigid links of the hoop assembly. The actuators are assumed to be placed so that the various modes indicated in Table 2 would be directly affected.

Table 2 - Relationship between actuators and modes directly influenced

Actuator no. (circled in Fig. 3)	Mode being affected
1 2 3 and 4	Feed Mast Torsion (12)
5	First Bending (about y axis) (8)
6	First Bending (about x axis) (9)
7	Surface Torsion (10)
8 (Torquer)	Yaw (rotation about z axis) and First Torsion (7)
9	Translation along x and 2nd mast bending (11)
10	Translation along y and 2nd mast bending (12)
11	Translation along z
12	Pitch (rotation about y axis)
13	Roll (rotation about x axis)

Possible sets of the minimum number of actuators include (1,2,3,4,5,12) and (8,9,10,11,12,13). On the contrary, the six actuators (1,2,3,4,6,7) are insufficient to control the thirteen system modes as states 14,15, and 26 in the digraph (Fig. 2) can not be reached from any of these six inputs (under the assumption that any element in the $\phi^T B$ matrix which is less than 10^{-5}, and six or seven orders of magnitude less than the maximum entry, is treated numerically equal to zero).

IV. Control Law Synthesis

Once controllability has been established control law design is based on: 1) application of the linear regulator problem from optimal control theory; and 2) pole allocation algorithms. The ORACLS[8] software package has been used to obtain the control law gains and generate the required time histories of the actuator forces as well as the dynamic transient responses.

1) Application of the Linear Regulator Problem

The control law of the form:

$$U = -FX \tag{9}$$

for the dynamical system

$$\dot{X} = AX+BU \tag{10}$$

is selected such that the following performance index is minimized[9]

$$J = \int_0^t (X^T QX+U^T RU)\, dt \tag{11}$$

where Q and R are positive semi-definite and positive definite weighting matrices, respectively.

The gain matrix, F, is given by:

$$F = R^{-1}B^T P \tag{12}$$

where P corresponds to the positive definite solution of the matrix Riccati differential equation:

$$-PA-A^T P+PBR^{-1}B^T P-Q = dP/dt \tag{13}$$

The steady state solution (as $t \to \infty$) of the Riccati matrix equation can be obtained by solving equation (13) after setting $dP/dt=0$. The steady state Riccati matrix solution results in a constant gain matrix which is relatively easy to implement as compared with the time varying solution of the matrix Riccati differential equation.

In order to guarantee controllability in the event that one of the actuators might fail, it was decided to select the minimum number of actuators in this study to be seven instead of the six previously discussed. For seven actuators assumed (actuator numbers 7 to 13 in Table 2) a parametric study was performed showing the effect of varying Q (100I to 10,000I) and R (I to 100I, where I is the appropriately dimensioned identity matrix) on the least damped mode of the closed-loop system (Fig. 4). It can be concluded that Q = 1000I and R=I is a reasonable operating (starting) point in the Q and R domain as the curve corresponding to R=I is relatively less sensitive to changes in Q as compared with other values of R.

As an example, Table 3 shows the effect of varying the number of actuators (from seven to thirteen) on the maximum force amplitude required of any single actuator for the same set of initial conditions in the modal coordinates and the same state and control weighting matrices. As indicated, the maximum peak force required of any actuator is reduced as the number of actuators is increased. The system transient performance is improved by increasing the number of actuators (Table 4), but at the expense of a slight increase in control effort. Other studies showing the effects of: (1) removing three of the rigid modes from the model; or (2) ignoring initial displacements in these modes, could result in overly optimistic results in terms of control system requirements (Tables 5 and 6).

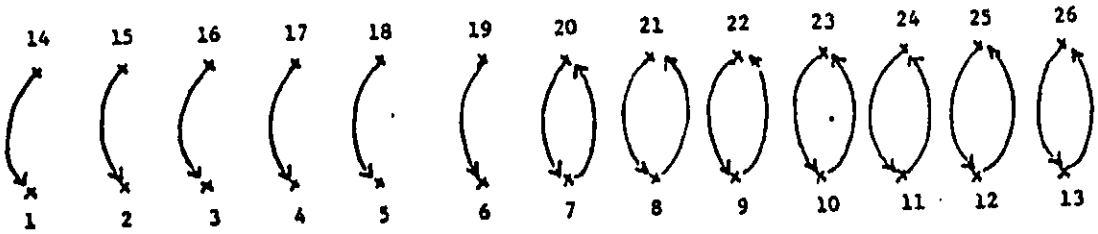

Fig. 2 Digraph of the system matrix.

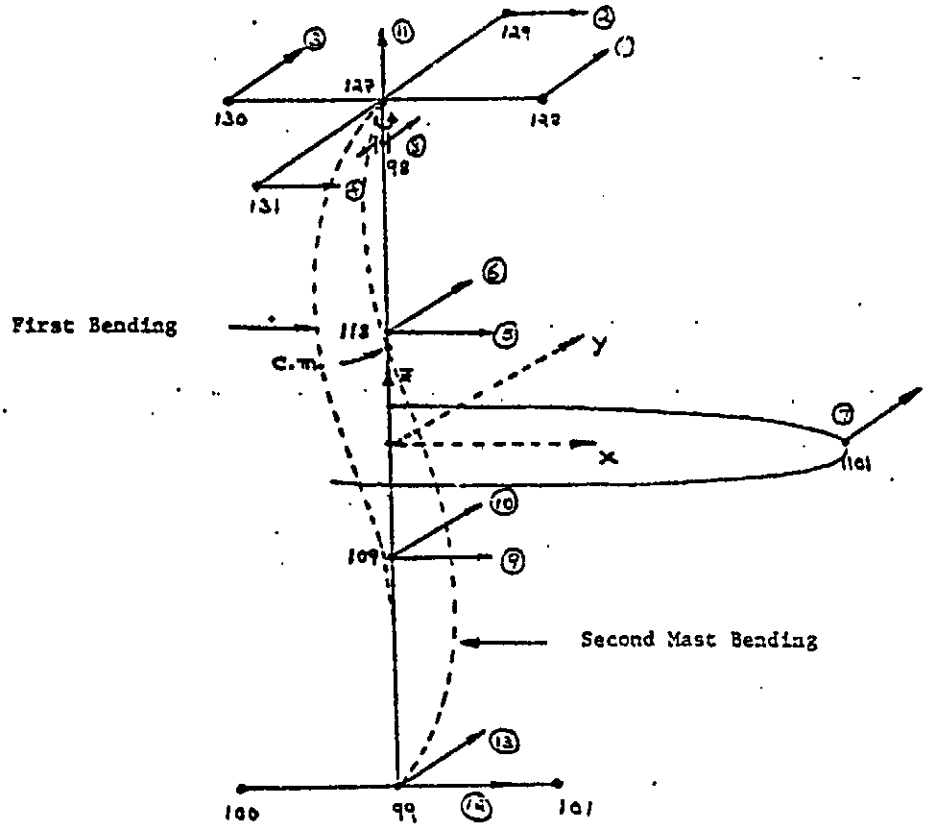

Fig. 3 Proposed arrangement of actuators Hoop/Column system.
(uncircled numbers identify grid points from finite element analysis)

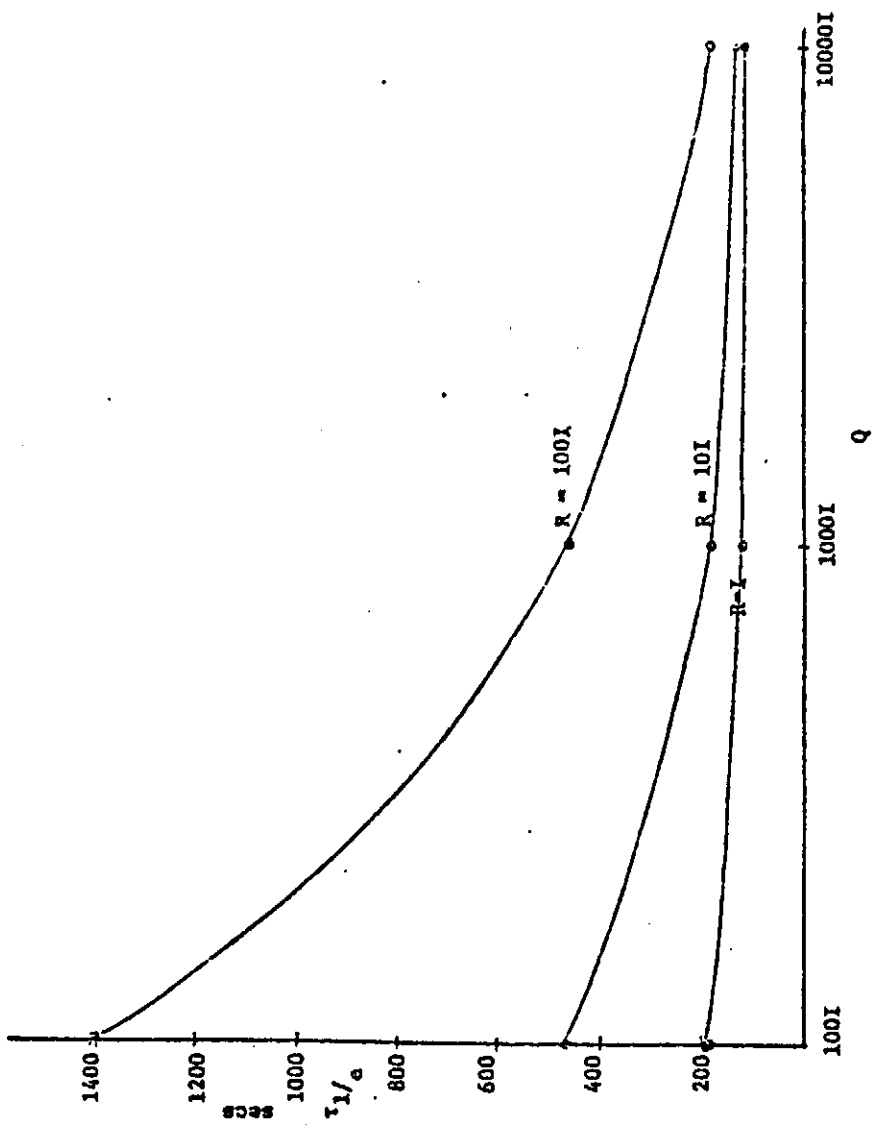

Fig. 4 Variation of the time constant of the least damped mode with Q and R penalty matrices.

Table 3 - Summary of maximum actuator forces(amplitudes) required
Hoop/Column - varying the no. of actuators (7-13)
Initial Condition: $q_i(0)=0.01$ i=1,2....13, Q=1000I, R=I

Max. Actuator Force Amplitudes Pounds		No. of Actuators						
		7	8	9	10	11	12	13
f_1								0.3500
f_2							0.1364	0.0569
f_3						0.3158	0.3357	0.3000
f_4					0.3251	0.2101	0.1364	0.0569
f_5				1.303	1.3029	1.3027	1.3027	1.3027
f_6			0.6632	0.6631	0.1831	0.2898	0.2847	0.2833
f_7		1.694	1.514	1.515	1.4734	1.2798	1.2781	1.2761
f_8	(in.-lb)	0.109	0.104	0.104	0.1004	0.0124	0.0117	0.0123
f_9		1.1891	1.1889	0.287	0.2276	0.2369	0.2369	0.2369
f_{10}		1.0602	0.7380	0.7380	0.1673	0.1601	0.1573	0.1573
f_{11}		0.4209	0.4089	0.4326	0.4199	0.4055	0.4061	0.4061
f_{12}		0.1208	0.1208	0.3521	0.3521	0.3521	0.3521	0.3521
f_{13}		0.2998	0.1866	0.1866	0.0669	0.0658	0.0673	0.0688

Table 4 - Comparison of closed loop poles - Hoop/Column with 7 and 13 actuators

Q = 1000I, R=I 13 modes

7 Actuators - Poles		13 Actuators - Poles	
σ-(Real)-1/sec	jω-(Imaginary)	σ-(Real)-1/sec	jω-(Imaginary)
-0.0077	5.5905	-0.008	5.5905
-0.0077	-5.5905	-0.008	-5.5905
-0.0100	0.7465	-0.7045	0.7788
-0.0100	-0.7465	-0.7045	-0.7788
-0.4343	0.4053	-0.4179	0.4544
-0.4343	-0.4053	-0.4179	-0.4544
-0.8578	1.7117	-2.1916	1.6704
-0.8578	-1.7117	-2.1916	-1.6704
-0.9035	2.7007	-0.9806	2.6637
-0.9035	-2.7007	-0.9806	-2.6637
-3.0979	1.666	-3.6151	1.7994
-3.0979	-1.666	-3.6151	-1.7994
-0.4689	1.3656	-1.0058	0
-0.4689	-1.3656	-1.0117	0
-0.5583	0.4892	-1.0247	0
-0.5583	-0.4892	-1.0260	0
-1.0059	0	-1.0868	0
-1.0226	0	-1.0987	0
-1.0287	0	-1.2914	0
-1.2830	0	-1.5808	0
-1.5977	0	-3.9913	0
-2.4285	0	-5.4766	0
-3.4251	0	-6.2706	0
-6.9508	0	-10.019	0
-11.8231	0	-12.424	0
-18.1405	0	-30.186	0

Table 5 - Comparison of maximum actuator force amplitudes
Q = 1000I, R=I, $q_i(0) = 0.01$,

Max. Actuator Force Amplitudes Pounds	13 Actuators/13 Modes	10 Actuators/10 Modes
f_1	0.3500	
f_2	0.0569	
f_3	0.3030	
f_4	0.0569	0.2514
f_5	1.3000	1.3759
f_6	0.2830	0.2850
f_7	1.2700	0.3713
f_8 (in-lb)	0.0124	0.0171
f_9	0.2360	0.4031
f_{10}	0.1570	0.2508
f_{11}	0.4060	0.1654
f_{12}	0.3520	0.2078
f_{13}	0.0688	0.4115

Table 6 - Comparison of maximum actuator force amplitudes
Q = 1000I, R=I 13 Actuators/13 Modes

Max. Actuator Force Amplitudes Pounds	$q_i(0)$=0.01, i=1,2...13	$q_i(0)$=0, i=1 to 6 $q_i(0)$=0.01, i=7 to 13
f_1	0.3500	0.3462
f_2	0.0569	0.0324
f_3	0.3030	0.2923
f_4	0.0569	0.0324
f_5	1.3000	0.9846
f_6	0.283	0.3021
f_7	1.2700	0.8423
f_8 (in.-lb)	0.0124	0.0124
f_9	0.236	0.1471
f_{10}	0.157	0.1566
f_{11}	0.406	0.0327
f_{12}	0.3520	0.0976
f_{13}	0.0688	0.0931

2) Application of the Pole Placement Algorithm

As an example of the application of the pole placement technique, Fig. 5 illustrates the transient response in key modal amplitudes, as well as required actuator force history for an initial condition only in the first torsional mode. The pole placement algorithm[8] requires that all of the poles be placed along a line parallel to the imaginary axis. It is seen that the requirement that each mode have a time constant of 100 secs, is a less stringent requirement on the control system than for the case depicted in Table 3 and 4 (13 actuators) where the most damped mode has a time constant of approximately 1/30 sec.

3) Effect of Removing Hoop Mounted Actuator

If the seventh actuator is removed from the system leaving a total of 12 working actuators, there is a deterioration in the lowest damped modal time constants. The magnitude of the real part of the least damped mode is reduced from 0.008 (Table 4) to 0.0024 and there are now ten poles with amplitudes of real parts less than 1.0. The maximum actuator forces required in response to initial displacements of 0.01 in all 13 modes are not greatly different from those shown in Table 3 for the case of 12 or 13 actuators.

On the other hand if a total of only seven actuators is now assumed ($f_{13}, f_{12}, f_{11}, f_{10}, f_9, f_8, f_6$) there is considerable loss of performance in the least damped mode. The least damped modal time constant has now increased to about 2000 sec as compared with 130 sec (as shown in Table 4). It should be noted that the least damped modes throughout this study correspond to both feed mast torsion and surface torsion. Again the maximum actuator forces required in response to initial displacements of 0.01 in all 13 modes are essentially the same order as shown in Table 3 for the case of seven actuators (including f_7).

Additional results explained in Ref.10, consider the effect of varying the elements in the state penalty matrix so that the modes with poorest transient characteristics would be penalized more. There appears to be some advantage in appropriately selecting the "split" weighting elements so as to improve performance in the lowest damped modes without unduly increasing the actuator-force requirements.

V. Concluding Comments

Generally, it can be concluded that the use of the graph theory enables the designer to have an intuitive qualitative idea about where actuators can be placed in order to achieve controllability. In most cases simulated, surface torsion and feed mast torsion are among modes having the longest time constants. Transient performance can be improved by appropriately changing the related elements in the state penalty matrices, but usually at the expense of control system effort. The linear quadratic Gaussian technique offers more flexibility to the controls designer in attempting to meet the performance requirements, while also maintaining propellant consumption at desired levels. System transient characteristics are degraded when the hoop-mounted actuator is not included. This degradation is more pronounced as the number of (remaining) actuators is reduced. The control efforts depicted here for the transient times considered appear reasonable in terms of the over-all system mass and surface and pointing requirement. Before meaningful conclusions can be made regarding RMS pointing and surface accuracy requirements the effects of both sensor and plant noise and also environmental disturbances should be incorporated into the existing model and are suggested for further study.

References

1. Golden, C.T., Lackey, J.A., and Spear, E.E., "Configuration Development of the Land Mobile Satellite System (LMSS) Spacecraft," Large Space Systems Technology-1981, Third Annual Technical Review, NASA Langley Research Center, Nov. 16-19, 1981, NASA Conference Publication 2215, Part 2, pp. 711-766.

2. Sullivan, M.R., "Maypole (Hoop/Column) Concept Development Program," Large Space Systems Technology-1981, Third Annual Technical Review, NASA Langley Research Center, Nov. 16-19, 1981, NASA Conference Publication 2215, Part 2, pp. 503-550.

3. Reddy, A.S.S.R. and Bainum, P.M., "Controllability of Inherently Damped Large Flexible Space Structures," 33rd International Astronautical Congress, Paris, Sept. 27-Oct. 2, 1982, Paper No. IAF 82-319; to appear, Acta Astronautica.

4. Bainum, P.M. and Reddy, A.S.S.R., "On the Shape and Orientation Control of an Orbiting Shallow Spherical Shell Structure," Joint IFAC/ESA Symposium on Automatic Control in Space, Noordwijkerhout, The Netherlands, July 5-9,1982.

5. Joshi, S.M., "Control System Synthesis for a Large Flexible Space Antenna," 33rd International Astronautical Congress, Paris, Sept. 27-Oct. 2, 1982, Paper No. IAF 82-320.

6. "The Versatile Hoop/Column Structural Dynamic Model," supplied by NASA Langley Research Center, 1982.

7. Balas, M.J., "Feedback Control of Flexible Systems," IEEE Trans. on Automatic Control, Vol. AC-23, No. 4, 1978, pp. 673-679.

8. Armstrong, E.S., "ORACLS - A System for Linear-Quadratic-Gaussian Control Law Design," NASA Technical Paper 1106, April 1978.

9. Bryson, A.E., Jr., and Ho, Y.C., Applied Optimal Control, Blaisdell Publishing Co., Waltham, Mass. 1969.

10. Bainum, P.M., Reddy, A.S.S.R., Krishna, R., and Diarra, C.M., "The Dynamics and Control of Large Flexible Space Structures-VI," Final Report: NASA Grant NSG-1414, Suppl. 5, Howard University, 1983.

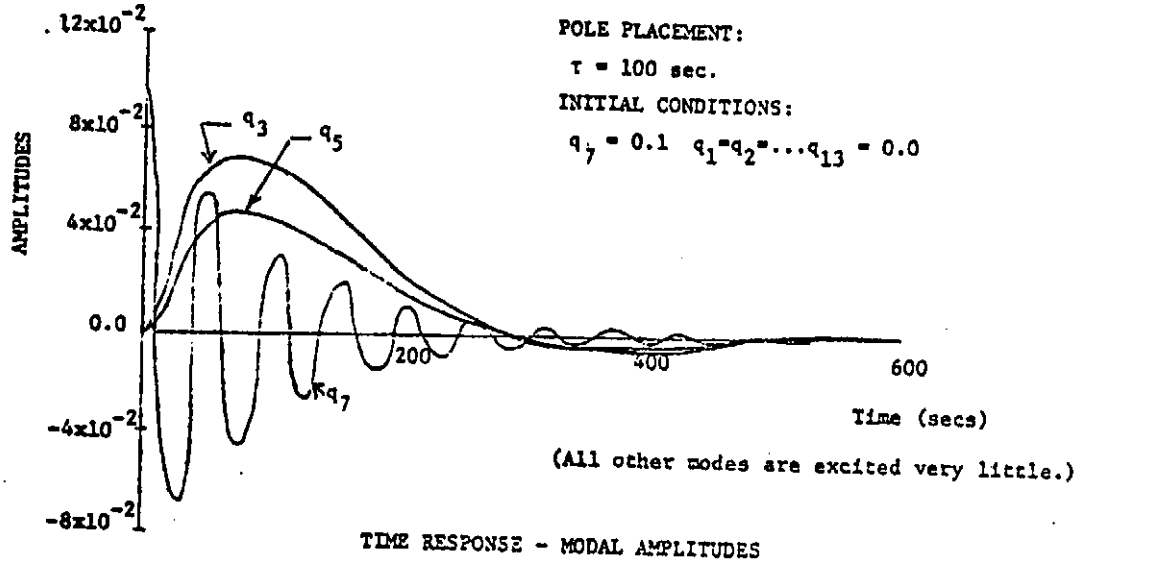

POLE PLACEMENT:

τ = 100 sec.

INITIAL CONDITIONS:

$q_7 = 0.1 \quad q_1 = q_2 = \ldots q_{13} = 0.0$

(All other modes are excited very little.)

TIME RESPONSE - MODAL AMPLITUDES

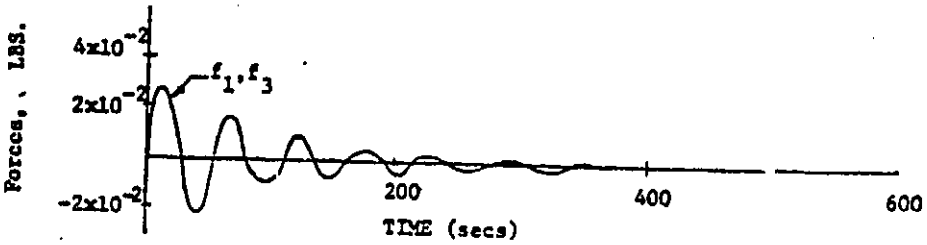

(Peak forces for all other actuators are far less)

Fig. 5 Pole placement - time response, modal amplitudes and required actuator force time history.

II.B ADDITIONAL RESULTS ON CONTROL LAW DESIGN FOR HOOP-COLUMN USING LINEAR QUADRATIC CONTROL THEORY

The concept of split weighting of different modes in the quadratic cost function is used to further penalize modes 7 (combinations of yaw and first torsion of the system), 10 (surface torsion), 12 (feed mast torsion) and their rates. These modes are penalized 10 times more than the rest of the modes and the resulting closed loop poles are tabulated in Table 7 together with the uniform weighting results. It is observed that the time constant of the least damped mode (-0.0120) for the case of split weighting is improved without increasing the most damped mode (-30.1864) as compared to the uniform weighting case. The effect of split weighting is also apparent in the maximum actuator force amplitude [Table 8], with the requirement of a slightly larger control effort.

The actuator of the hoop (#7) is then removed; for the values of $Q = 1000\ I$ and $R = I$ the closed loop poles are compared with those for the case with the actuator on the hoop in Table 9. The corresponding required actuator forces are given in Table 10. The closed loop poles with the hoop actuators removed for a total of 7, 10, and 12 actuators, respectively, and with: $Q = 1000\ I$, $R = I$; $Q = 10{,}000\ I$, $R = I$; and $Q = 100{,}000\ I$, $R = I$; are given in Tables 11, 12 and 13. The split weighting case is also considered and the corresponding closed loop poles are given in Table 14. The maximum actuator forces for the various cases described above are given in Tables 15, 16, and 17.

To have an understanding of the relation between the actual coordinates and the modal coordinates (as the complete eigenvector matrix is not available) certain initial conditions are assumed for the modal

coordinates (q_i, i=1, --13) and the corresponding displacements are calculated. The nodes that experience maximum displacements together with the values of the displacements are shown in Table 18. It can be seen that nodes 100 and 101 have experienced the maximum displacements for the various initial conditions assumed for the modal coordinates. The general conclusions for the various cases described so far are enumerated below.

1. As the number of actuators is increased, for a given set of initial conditions, the maximum force amplitude required for any actuator is, in general, reduced.

2. In general, by increasing all elements in the Q matrix in the same relative amount, transient performance in the least damped modes is improved, but at the expense of a larger control effort.

3. Split weighting of appropriate elements in the Q matrix can result in improved transient performance without unduly increasing the control effort.

4. System transient characteristics are degraded when the hoop mounted actuator is not included. Degradation is more pronounced as the number of (remaining) actuators is reduced.

5. For most cases simulated surface torsion and feed mast torsion are among modes with largest time constants.

6. For the same initial displacements in each of the 13 modal coordinates, it is seen that the maximum translational displacements are realized at nodes 100, 101 (at the ends of the lower solar panels).

Table 7

COMPARISON OF CLOSEDLOOP POLES HOOP/COLUMN 13 ACTUATORS-13 MODES

13 Actuators Poles Q=1000I, R=I		13 Actuators Poles Q=1000I Except Q(7,7)=Q(10,10)=Q(12,12) =Q(20,20)=Q(22,22)=Q(25,25)= 10000I, R=I	
(Real)	jw(Imaginary)	(Real)	jw(Imaginary)
-0.0080	5.5905	-0.0120	5.5905
-0.0080	-5.5905	-0.0120	-5.5905
-0.7045	0.7788	-0.4179	0.4545
-0.7045	-0.7788	-0.4179	-0.4545
-0.4179	0.4544	-1.0922	1.5579
-0.4179	-0.4544	-1.0922	-1.5579
-2.1916	1.6704	-2.1916	1.6704
-2.1916	-1.6704	-2.1916	-1.6704
-0.9806	2.6637	-3.6157	1.7991
-0.9806	-2.6637	-3.6157	-1.7991
-3.6151	1.7994	-1.0055	0
-3.6151	-1.7994	-1.0120	0
-1.0058	0	-1.0250	0
-1.0117	0	-1.0260	0
-1.0247	0	-1.0864	0
-1.0260	0	-1.0987	0
-1.0868	0	-1.1993	0
-1.0987	0	-1.2903	0
-1.2914	0	-1.5844	0
-1.5808	0	-2.5898	0
-3.9913	0	-3.9914	0
-5.4766	0	-5.4866	0
-6.2706	0	-6.3240	0
-10.0190	0	-10.0617	0
-12.4240	0	-25.4183	0
-30.1860	0	-30.1864	0

Table 8

COMPARISON OF MAXIMUM ACTUATOR FORCES HOOP/COLUMN 13 ACTUATORS-
13 MODES

Max. Actuator Forces (Amp.)-Pounds	13 Actuators 13 Modes Qi(0)=0.01,i=1,..,13 Q=1000I, R=I	13 Actuators 13 Modes Qi(0)=0.01,i=1,..,13 Q=1000I, Except Q(7,7)=Q(10,10)= Q(12,12)=Q(20,20)= Q(22,22)=Q(25,25)= 10000I, R=I
f(1)	0.3500	1.7450
f(2)	0.0569	0.0061
f(3)	0.3000	1.7380
f(4)	0.0569	0.0061
f(5)	1.3027	1.3029
f(6)	0.2833	0.7383
f(7)	1.2761	2.3580
f(8) (ft-lb)	0.0123	0.0817
f(9)	0.2369	0.2277
f(10)	0.1570	0.1693
f(11)	0.4061	0.4178
f(12)	0.3521	0.3521
f(13)	0.0688	0.0978

Table 9

COMPARISON OF CLOSEDLOOP POLES HOOP/COLUMN 12/13 ACTUATORS
Q=1000I,R=I

13 Mode Model 13 Actuator-Poles		13 Mode Model W.O Actuator7 12 Actuator-Poles	
(Real)	jw(Imaginary)	(Real)	jw(Imaginary)
-0.008	5.5905	-0.0024	5.5905
-0.008	-5.5905	-0.0024	-5.5905
-0.7045	0.7788	-0.0162	3.1813
-0.7045	-0.7788	-0.0162	-3.1813
-0.4179	0.4544	-0.2654	0.5653
-0.4179	-0.4544	-0.2654	-0.5658
-2.1916	1.6704	-0.4179	1.6704
-2.1916	-1.6704	-0.4179	-1.6704
-0.9806	2.6637	-0.9173	1.7994
-0.9806	-2.6637	-0.9173	-1.7994
-3.6151	1.7994	-2.1916	0
-3.6151	-1.7994	-2.1916	0
-1.0058	0	-3.6153	0
-1.0117	0	-3.6153	0
-1.0247	0	-1.0117	0
-1.0260	0	-1.0247	0
-1.0868	0	-1.0258	0
-1.0987	0	-1.0859	0
-1.2914	0	-1.0987	0
-1.5808	0	-1.2785	0
-3.9913	0	-1.6052	0
-5.4766	0	-3.9913	0
-6.2705	0	-5.4867	0
-10.019	0	-6.3275	0
-12.424	0	-10.0673	0
-30.186	0	-30.1860	0

Table 10

COMPARISON OF ACTUATOR FORCES VARYING THE ACTUATORS WITH SEVENTH ACTUATOR REMOVED

Q=1000I, R=I

Max. Act. Forces(Amp) lbs	7 Actuators	10 Actuators	12 Actuators
f(1)	1.4019	1.9990	1.5187
f(2)	0.4491	0.5261	0.0176
f(3)	1.1869	1.3024	1.5298
f(4)	0.3411	0.5685	0.0176
f(5)	0.3612	0.0636	1.3024
f(6)	0.1209	0.2369	0.5597
f(7)			
f(8) lb.ft	0.2296	0.2047	0.0423
f(9)		0.3603	0.2279
f(10)		0.3520	0.1695
f(11)		0.1072	0.3686
f(12)			0.3520
f(13)			0.0789

Table 11

COMPARISON OF CLOSEDLOOP POLES HOOP/COLUMN SYSTEM WITH SEVENTH ACTUATOR ON HOOP REMOVED- 13 MODES Q=1000I, R=I

7 Actuators (real)	jw(Imaginary)	10 Actuators (Real)	jw(Imaginary)	12 Actuators (Real)	jw(Imaginary)
-0.0004	5.5905	-0.0016	5.5905	-0.0024	5.5905
-0.0004	-5.5905	-0.0016	-5.5905	-0.0024	-5.5905
-0.0007	3.1813	-0.0010	3.1813	-0.0162	3.1813
-0.0007	-3.1813	-0.0010	-3.1813	-0.0162	-3.1813
-0.0063	0.7467	-0.3084	0.6657	-0.2654	0.5678
-0.0063	-0.7467	-0.3084	-0.6657	-0.2654	-0.5678
-0.0434	0.0433	-0.4179	0.4544	-0.4179	0.4544
-0.0434	-0.0433	-0.4179	-0.4544	-0.4179	-0.4544
-0.4343	0.4053	-0.4505	0.4712	-0.9173	0.5968
-0.4343	-0.4053	-0.4505	-0.4712	-0.9173	-0.5968
-0.4690	1.3656	-2.1916	1.6704	-2.1916	1.6704
-0.4690	-1.3656	-2.1916	-1.6704	-2.1916	-1.6704
-0.5243	0.5476	-3.6515	1.8369	-3.6153	1.7994
-0.5243	-0.5476	-3.6515	-1.8369	-3.6153	-1.7994
-3.5693	1.8674	-1.0150	0	-1.0117	0
-3.5693	-1.8674	-1.0247	0	-1.0247	0
-1.0180	0	-1.0365	0	-1.0258	0
-1.0287	0	-1.0907	0	-1.0858	0
-1.0681	0	-1.0987	0	-1.0987	0
-1.2746	0	-1.2839	0	-1.2785	0
-1.6147	0	-1.5947	0	-1.6052	0
-2.4285	0	-3.9913	0	-3.9913	0
-3.4220	0	-3.9989	0	-5.4867	0
-6.0668	0	-6.1550	0	-6.3275	0
-10.656	0	-10.661	0	-10.067	0
-18.141	0	-30.186	0	-30.186	0

Table 12

COMPARISON OF CLOSEDLOOP POLES HOOP/COLUMN SYSTEM WITH SEVENTH ACTUATOR REMOVED 13 MODES Q=10000I, R=I

7 Actuators		10 Actuators		12 Actuators	
(Real)	jw(Imaginary)	(Real)	jw(Imaginary)	(Real)	jw(Imaginary)
-0.0005	5.5905	-0.0038	5.5905	-0.0062	5.5905
-0.0005	-5.5905	-0.0038	-5.5905	-0.0062	-5.5905
-0.0008	3.1813	-0.0230	3.1812	-0.0329	3.1809
-0.0008	-3.1813	-0.0230	-3.1812	-0.0329	-3.1809
-0.0113	0.7467	-0.2550	0.5623	-0.2497	0.5597
-0.0113	-0.7467	-0.2550	-0.5623	-0.2497	-0.5597
-0.0774	0.7693	-0.5012	0.5193	-0.5012	0.5193
-0.0774	-0.7693	-0.5012	-0.5193	-0.5012	-0.5193
-0.4855	0.5466	-1.3077	0.4208	-1.0011	0
-0.4855	-0.5466	-1.3077	-0.4208	-1.0023	0
-0.6087	0.1463	-1.0014	0	-1.0023	0
-0.6087	-0.1463	-1.0023	0	-1.0081	0
-0.6476	0.6713	-1.0033	0	-1.0086	0
-0.6476	-0.6713	-1.0085	0	-1.0124	0
-1.0017	0	-1.0086	0	-1.0549	0
-1.0026	0	-1.0125	0	-1.3041	0
-1.0062	0	-1.3041	0	-1.9257	0
-1.0124	0	-1.3215	0	-3.7535	0
-1.0924	0	-6.3906	0	-6.4064	0
-1.2619	0	-8.7613	0	-8.7613	0
-6.4271	0	-11.895	0	-12.655	0
-12.387	0	-13.193	0	-13.193	0
-13.099	0	-14.993	0	-19.119	0
-27.282	0	-27.292	0	-27.313	0
-34.811	0	-34.828	0	-34.853	0
-62.659	0	-98.551	0	-98.551	0

Table 13

COMPARISON OF CLOSEDLOOP POLES HOOP/COLUMN SYSTEM WITH SEVENTH ACTUATOR ON HOOP REMOVED 13 MODES Q=100000I, R=I

7 Actuators		10 Actuators		12 Actuators	
(Real)	jw(Imaginary)	(Real)	jw(Imaginary)	(Real)	jw(Imaginary)
-0.0007	5.5905	-0.0079	5.5905	-0.0096	5.5905
-0.0007	-5.5905	-0.0079	-5.5905	-0.0096	-5.5905
-0.0011	3.1813	-0.0369	3.1807	-0.0399	3.1806
-0.0011	-3.1813	-0.0369	-3.1807	-0.0399	-3.1806
-0.0314	0.7468	-0.2488	0.5592	-0.2483	0.5590
-0.0314	-0.7468	-0.2488	-0.5592	-0.2483	-0.5590
-0.1383	0.1358	-0.5429	0.5572	-0.5249	0.5572
-0.1383	-0.1358	-0.5429	-0.5572	-0.5249	-0.5572
-0.4809	0.5699	-1.0001	0	-1.0001	0
-0.4809	-0.5699	-1.0002	0	-1.0002	0
-0.6212	1.4837	-1.0003	0	-1.0002	0
-0.6212	-1.4837	-1.0008	0	-1.0008	0
-0.6585	0.7347	-1.0009	0	-1.0009	0
-0.6585	-0.7347	-1.0012	0	-1.0012	0
-1.0000	0	-1.0211	0	-1.0047	0
-1.0002	0	-1.0293	0	-1.0293	0
-1.0006	0	-1.0357	0	-1.0349	0
-1.0013	0	-5.9089	0	-12.513	0
-1.0085	0	-20.438	0	-20.487	0
-1.0232	0	-28.795	0	-28.795	0
-20.551	0	-37.884	0	-40.434	0
-39.367	0	-41.900	0	-41.900	0
-41.914	0	-47.751	0	-60.609	0
-88.147	0	-88.174	0	-88.248	0
-110.47	0	-110.53	0	-110.60	0
-199.66	0	-312.59	0	-312.59	0

Table 14

COMPARISON OF CLOSEDLOOP POLES HOOP/COLUMN SYSTEM WITH SEVENTH ACTUATOR REMOVED 13 MODES Q=1000I EXCEPT Q(7,7)=Q(10,10)=Q(12,12) =Q(20,20)=Q(22,22)=Q(25,25)=10000I, R=I

7 Actuators		10 Actuators		12 Actuators	
(Real)	jw(Imaginary)	(Real)	jw(Imaginary)	(Real)	jw(Imaginary)
-0.0013	5.5905	-0.0050	5.5905	-0.0068	5.5905
-0.0013	-5.5905	-0.0050	-5.5905	-0.0068	-5.5905
-0.0024	3.1813	-0.0277	3.1811	-0.0381	3.1808
-0.0024	-3.1813	-0.0277	-3.1811	-0.0381	-3.1808
-0.0200	0.7467	-0.2389	0.3015	-0.2367	0.3100
-0.0200	-0.7467	-0.2389	-0.3015	-0.2367	-0.3100
-0.0434	0.0433	-0.4179	0.4544	-0.4179	0.4544
-0.0434	-0.0433	-0.4179	-0.4544	-0.4179	-0.4544
-0.4343	0.4053	-0.9883	0.6871	-2.1916	1.6704
-0.4343	-0.4053	-0.9883	-0.6871	-2.1916	-1.6704
-0.4690	1.3656	-2.1916	1.6704	-3.6158	1.7991
-0.4690	-1.3656	-2.1916	-1.6704	-3.6158	-1.7991
-0.5240	0.5478	-3.6401	1.8295	-1.0017	0
-0.5240	-0.5478	-3.6401	-1.8295	-1.0247	0
-3.5693	1.8675	-1.0150	0	-1.0258	0
-3.5693	-1.8675	-1.0248	0	-1.0853	0
-1.0180	0	-1.0349	0	-1.0987	0
-1.0287	0	-1.0879	0	-1.1684	0
-1.0680	0	-1.0987	0	-1.2852	0
-1.2750	0	-1.2831	0	-1.5958	0
-1.6150	0	-1.5966	0	-2.6473	0
-2.4280	0	-3.9914	0	-3.9913	0
-3.4220	0	-4.3071	0	-5.4889	0
-6.0669	0	-6.1674	0	-6.3662	0
-10.066	0	-10.661	0	-10.673	0
-18.141	0	-30.186	0	-30.186	0

Table 15

COMPARISON OF ACTUATOR FORCES VARYING THE ACTUATORS WITH SEVENTH ACTUATOR REMOVED

Q=10000I, R=I

Max. Act. Forces(Amp) lbs	7 Actuators	10 Actuators	12 Actuators
f(1)	4.0402	4.4356	3.5095
f(2)	3.3862	3.5324	0.0958
f(3)	4.3702	3.6011	3.3440
f(4)	2.8451	1.4979	0.0958
f(5)	1.1247	0.2639	3.6010
f(6)	0.2136	0.8500	1.2351
f(7)			
f(8) lb.ft	1.2184	0.6595	0.1721
f(9)		1.1955	0.8503
f(10)		0.9438	0.6543
f(11)		0.3166	1.1675
f(12)			0.9437
f(13)			0.2844

Table 16

COMPARISON OF ACTUATOR FORCES VARYING THE ACTUATORS WITH SEVENTH ACTUATOR REMOVED

Q=100000I, R=I

Max. Act. Forces(Amp) lbs	7 Actuators	10 Actuators	12 Actuators
f(1)	9.6904	8.4849	6.5981
f(2)	20.7948	8.6722	4.5791
f(3)	14.6512	1.1022	5.6822
f(4)	8.8780	3.5757	0.4579
f(5)	3.5327	1.4109	1.1023
f(6)	1.2470	3.3063	3.1263
f(7)			
f(8) lb.ft	4.1667	2.7808	1.2149
f(9)		3.9409	3.3061
f(10)		2.4642	2.8507
f(11)		1.0831	3.9445
f(12)			2.4643
f(13)			1.0771

Table 17

Q=1000I, EXCEPT Q(7,7)=Q(10,10)=Q(12,12)=Q(20,20)=Q(22,22)=Q(25,25)=10000I, R=I

Max. Act. Forces(Amp) lbs	7 Actuators	10 Actuators	12 Actuators
f(1)	3.0869	4.9872	3.5906
f(2)	1.2538	1.1888	0.0696
f(3)	1.1868	1.3020	3.6637
f(4)	1.4440	1.5255	0.0696
f(5)	0.3660	0.2012	1.3022
f(6)	0.1209	0.2367	1.2361
f(7)			
f(8) lb.ft	0.5030	0.2294	0.1461
f(9)		0.3169	0.2369
f(10)		0.3520	0.1751
f(11)		0.2888	0.3452
f(12)			0.3520
f(13)			0.1141

Table 18

RELATIONSHIP BETWEEN DISPLACEMENT IN THE MODAL COORDINATES AND MAXIMUM TRANSLATIONAL DISPLACEMENT (AT NODE 101)

Node	Intl. Condition Qi(0)	Max. translational Disp.-Inches
(100) 101	0.01	(0.2840) 0.3009
(100) 101	0.02	(0.5680) 0.6019
(100) 101	0.03	(0.8519) 0.9029
(100) 101	0.04	(1.1359) 1.2039
(100) 101	0.05	(1.4199) 1.5048
(100) 101	0.06	(1.7039) 1.8058
(100) 101	0.07	(1.9878) 2.1068
(100) 101	0.08	(2.2718) 2.4078
(100) 101	0.09	(2.5558) 2.7087
(100) 101	0.10	(2.8398) 3.0097

III. ORIENTATION AND SHAPE-CONTROL OF AN ORBITING FLEXIBLE BEAM UNDER THE INFLUENCE OF SOLAR RADIATION PRESSURE

In this paper, the uncontrolled and controlled dynamics of a thin flexible beam in orbit and in the presence of solar radiation disturbance are analyzed. A beam nominally oriented along (i) the local horizontal and carrying a gimballed rigid dumbbell for gravity stabilization, and (ii) a beam nominally oriented along the local vertical are considered. The uncontrolled dynamics of the beam in the presence of the solar radiation pressure disturbance shows the excitation of the rigid pitch mode. The control laws previously designed for the case where the environmental effects were neglected, are found to be inadequate to control the shape and orientation of very flexible beams that are exposed to solar radiation disturbances. The control laws and the gain parameters are reevaluated for both cases of nominal beam orientations; this results, in general, in increased robustness of the closed-loop system. Methods of obtaining a robust control system in the presence of environmental perturbations are discussed.

INTRODUCTION

At the operational altitudes of proposed future missions involving large space structures, the principal environmental disturbance will, in general, be due to solar radiation pressure. Solar pressure torques, induced on the structure, are dependent on the surface properties and the surface geometry.[1] Expressions for the induced solar pressure

torques on a free-free flexible beam were developed earlier.[2] The uncontrolled dynamics of a thin flexible beam in orbit under the influence of solar radiation pressure forces were considered for two cases of beam orientations, namely, (i) nominally oriented along the local vertical and (ii) nominally oriented along the local horizontal and gravity-stabilized using a rigid dumbbell attached at the center of mass of the beam. The uncontrolled and controlled dynamics for the two cases of nominal beam orientations have also been considered previously but in the absence of environmental disturbances.[3,4]

The objective of the present study is to evaluate the validity of the previously developed control laws, which were obtained disregarding the environmental effects, for controlling the shape and orientation of a beam actually under the influence of solar radiation disturbance. It is proposed to evaluate the robustness of the previously developed control laws for the beam under the influence of the solar pressure disturbances by considering a parametric study of the controlled dynamics for various initial conditions. Particular attention will be given to highly flexible structures under larger initial displacements. The feedback gains will be modified, where required, to achieve satisfactory transient performance while minimizing control force effort. Where modification of gain values are found not effective, modification of control laws and reselection of actuators and their locations will be considered.

THE MATHEMATICAL MODELLING OF A FLEXIBLE ORBITING BEAM

Dumbbell Stabilized Flexible Beam in Orbit Nominally Oriented Along the Local Horizontal

A flexible orbiting beam nominally oriented along the local horizontal represents a gravitationally unstable configuration. A passive stabilization of the beam can be obtained by using a rigid dumbbell with proper moment of inertia. In Ref. 3, the equations of motion for a beam with a dumbbell assumed to be attached at the center of mass of the beam (Fig. 1a) through a spring loaded hinge and with viscous rotational damping have been developed. It is assumed that the dumbbell mass is concentrated at the tips, that the viscous force at the hinge is linear, and that all displacements and deformations occur within the orbital plane. With the usual assumptions of small pitch amplitude and dumbbell oscillations and flexural deformations, the linearized equations of motion are obtained as[3],

$$\theta''+\bar{c}\theta'+(\bar{k}-3)\theta-\bar{c}\alpha'-\bar{k}\alpha+\sum_n(\bar{c}\varepsilon_n'+\bar{k}\varepsilon_n)C_z^{(n)}=C_y/J_y\omega_c^2 \tag{1}$$

$$\alpha''+c_1\bar{c}\alpha'+(c_1\bar{k}+3)\alpha-c_1\bar{c}\theta'-c_1\bar{k}\theta-\sum_n(\bar{c}\varepsilon_n'+\bar{k}\varepsilon_n)c_1C_z^{(n)}=0 \tag{2}$$

$$\varepsilon_n''+(\Omega_n^2-3)\varepsilon_n-\{\bar{k}(\alpha-\theta)+\bar{c}(\alpha'-\theta')\}C_z^{(n)}J_y/M_n\ell^2+\sum_m(\bar{c}\varepsilon_m'+\bar{k}\varepsilon_m)C_z^{(mn)}$$
$$=E_n/M_n\omega_c^2\ell \tag{3}$$

where $C_z^{(mn)} = J_y C_z^{(m)} C_z^{(n)} / M_n \ell^2$; (m,n = 1,2,...) and M_n = n^{th} modal mass

ℓ = undeformed beam length

θ = pitch angle

ω_c = orbital angular velocity

C_y = external torque about the pitch axis

J_y = beam pitch axis moment of inertia

A_n = n^{th} flexural modal amplitude

ε_n = A_n/ℓ, nondimensionalized n^{th} flexural modal amplitude

$\bar{k}$ = $k/J_y\omega_c^2$; $\bar{c}$ = $c/J_y\omega_c$

k = torsional restoring spring constant at the hinge

c = viscous damping coefficient

α = angle between the dumbbell axis and the local vertical

$$C_z^{(n)} = \frac{\partial \phi_z^{(n)}}{\partial x}\Big|_{x=0}$$

$\phi_z^{(n)}$ = beam shape function of the n^{th} transverse mode

c_1 = J_y/I_d, I_d = pitch moment of inertia of the dumbbell

Ω_n = ω_n/ω_c ; ω_n = n^{th} natural frequency

$( )'$ = $d/d\tau$ where $\tau = \omega_c t$

t = time

The following observations can be made from a study of Eqs. (1),(2) and (3) in the absence of external forces on the system: (a) the pitch motion of the beam, the dumbbell motion (α), and the elastic motion of the beam (ε_n) are all coupled to each other; (b) within the linear range the elastic modes for which $C_z^{(n)} = 0$ (the symmetric modes), are completely independent of the pitch and dumbbell motions. Furthermore these modes do not influence either the pitch or the dumbbell motion.

A Flexible Beam in Orbit Nominally Oriented Along the Local Vertical

The equations of motion for a thin uniform flexible beam in orbit with its axis nominally along the local horizontal (Fig. 1b) are developed in Ref. 3 and represent a gravitationally stable system. With the assumptions of small transverse in-plane vibrations and small amplitude pitch oscillations of the beam, the linearized equations of motion are obtained as[3],

$$\theta'' + 3\theta = C_y/J_y\omega_c^2 \qquad (4)$$

$$\varepsilon_n'' + \Omega_n^2 \varepsilon_n = E_n/M_n\omega_c^2\ell \qquad (5)$$

Active control is required to maintain the pitch orientation of the beam and to damp out the modal oscillations in the presence of the environmental disturbances. A point actuator located at one end of the beam is considered for shape and orientation control of both the dumbbell stabilized beam and the beam oriented along the local vertical. The development of the forcing terms on the right hand side of Eqs. (1)-(5), due to the solar radiation pressure is reviewed in the next section.

SOLAR RADIATION DISTURBANCE MODEL

A detailed study of the effect of solar radiation disturbance on the uncontrolled dynamics of a flexible beam appears in Ref. 2 and a summary of the disturbance model obtained is given below. Fig. 2 shows the geometry of reflection of a flexible beam vibrating in one of the free beam modes and exposed to solar radiation pressure. The incidence solar radiation vector, $\bar{\tau}$, and the unit normal to the surface, $\bar{n}$, are assumed to be in the plane of the transverse vibration of the beam. Then, $\bar{\tau}$ and $\bar{n}$ can be expressed as

$$\bar{\tau} = a_o\bar{I} + c_o\bar{K} \tag{6}$$

$$\bar{n} = (\phi'\bar{I}-\bar{K})/\sqrt{1+\phi'^2} \tag{7}$$

where, $\phi' = d\phi/d\xi$, ϕ is the free-free beam shape function and ξ is the nondimensionalized longitudinal coordinate of the beam.

The solar radiation force, $\bar{F}_a$, and moment, $\bar{N}_a$, acting on a completely absorbing surface is given by[1]

$$\bar{F}_a = h_o\bar{\tau}\int_s \bar{\tau}\cdot\bar{n}\, ds \tag{8}$$

$$\bar{N}_a = -h_o\bar{\tau}\times\int_s \bar{R}(\bar{\tau}\cdot\bar{n})\, ds \tag{9}$$

where $h_o = 4.64\times10^{-6}$ Nt/m^2 is a constant for earth orbiting spacecraft. The integration over the area, s, is bounded by the condition

$$\bar{\tau}\cdot\bar{n} \geq 0 \tag{10}$$

The corresponding force and moments for a completely reflecting surface are given by

$$\bar{F}_r = -2h_o\int_s \bar{n}(\bar{\tau}\cdot\bar{n})^2\, ds \tag{11}$$

$$\bar{N}_r = 2h_o\int_s \bar{n}\times\bar{R}(\bar{\tau}\cdot\bar{n})^2\, ds \tag{12}$$

where $\bar{R}$ is the position vector of ds with respect to the center of mass of the beam. For a surface with an arbitrary reflection

coefficient, ε_r, the force and moment expressions become[1]:

$$\bar{F}_{\varepsilon r} = \bar{F}_a + \varepsilon_r(\bar{F}_r - \bar{F}_a) \tag{13}$$

$$\bar{N}_{\varepsilon r} = \bar{N}_a + \varepsilon_r(\bar{N}_r - \bar{N}_a) \tag{14}$$

Only the moment expressions are of importance in analyzing the attitude motion of the beam. The expressions for the moments per unit width of the beam are developed using Eqs. (6) and (7) in Eqs. (9) and (12) as[2]:

$$\bar{N}_a = -h_o a_o c_o \delta_o \text{ (for symmetric modes)}$$

$$= 0 \qquad \text{(for asymmetric modes)} \tag{15}$$

$$\bar{N}_r = -2h_o \int_o^1 \frac{(a_o\phi' - c_o)^2}{(1+\phi'^2)} \{ \phi'\phi + (\xi - \tfrac{1}{2}) \} \, d\xi \, \bar{J} \tag{16}$$

The numerical integration of Eq. (16) has shown that the moment due to any asymmetric mode of the beam is extremely small as compared with the magnitudes for the symmetric modes and the moments, $\bar{N}_r$, due to the symmetric modes can be expressed in the form (similar to Eq. (15)),

$$\bar{N}_r \propto a_o c_o \delta_o \text{ (for the symmetric modes)} \tag{17}$$

Eq. (17) is valid for all symmetric modes and for small deflections of the beam. Eqs. (15) and (17) are used in Eq. (14) to obtain the total moment due to solar radiation pressure on a beam with a coefficient of reflectivity, ε_r. Further, the deflection at one end of the vibrating beam for a given mode can be written as

$$\delta_n(t) = \varepsilon_n(t) \, \ell$$

Thus, the total moment on the beam due to any one of the symmetric modes of the beam can be expressed as

$$N(t) = \varepsilon_n(t) \, \ell \, N_m \, a_o c_o \tag{18}$$

where $a_o = \sin\theta_i$ and $c_o = \cos\theta_i$ and θ_i is the solar incidence angle given by[2]

$$\theta_i(t) = \omega_c t + \theta(t) + \theta_i(0) \tag{19}$$

Where ω_c = orbital angular velocity

$\theta(t)$ = pitch angle of the beam.

The effect of the disturbance on the generic mode is obtained by evaluating the integral[5]

$$E_n = \int \bar{\phi}^{(n)} (\xi) \cdot \bar{F} \, ds \tag{20}$$

where, $\bar{F}$ is the external force due to solar pressure. Eqs. (8) and (11) are substituted into Eq. (20) and the resulting integrals are evaluated under small amplitude approximations with the result that,[2]

$$E_{n_a} = E_{n_r} = 0$$

$$\text{and} \quad E_n = E_{n_a} + \epsilon_r (E_{n_r} - E_{n_a}) = 0 \tag{21}$$

Thus, the principal effect of solar radiation pressure on the flexible beam is to produce a net moment about the pitch axis of the beam. For a beam of length 100m and $\epsilon_r = 0.5$, the maximum pitch moment per unit deflection, N_m, in Eq. (18) is obtained using Eqs. (14), (15) and (16) as,[2]

$$N_m = 2.23\times10^{-4} + 0.5(9.4\times10^{-5} - 2.23\times10^{-4})$$

$$= 1.58\times10^{-4} \text{ Nt-m}$$

(N_m calculated here is for a beam with unit width). Eq. (18) is now ready to be used as the pitch forcing function in Eqs. (1) and (4).

CONTROL OF THE ORBITING BEAM SYSTEM

For applications of control theory the sets of second order equations, Eqs. (1)–(3), and (4) and (5) are transformed into a state vector form given by

$$\dot{X} = AX + BU + D \tag{22}$$

where X is the state vector of order (2m), m is the total number of rigid and flexible modes in the system. The plant matrix has dimensionality (2mx2m), B, (2mxr), where r denotes the number of actuators and D is a vector of order 2m denoting the disturbance and is a function of both time and the state of the system. For the dumbbell stabilized beam with two flexible modes included in the model, the order of the system will be 8, and for the beam oriented along the local vertical the order of the system with the two flexible modes, will be 6.

A single point actuator located at one end of the beam was considered for both cases of the beam's nominal orientation in Ref. 4. An ideal feedback law of the form $U = -KX$ is assumed to obtain a control law and the corresponding gain values, K. In the following sections the control problem is considered separately for the two cases of the beam orientation.

Control of the Dumbbell Stabilized Flexible Beam

The disturbance due to the solar radiation effects on the dumbbell is neglected in the following study, since the dumbbell is assumed to be rigid. The solar radiation disturbance vector, D, is then given by

$$D = [0,0,0,\ N/J\omega_c^2\ell,\ 0,0,0]^T \tag{23}$$

and

$$N = \varepsilon_1 \ell\, N_m \sin\theta_1 \cos\theta_1 \quad \text{(from Eq. 18)} \tag{24}$$

In the absence of both the control and the disturbance, an initial displacement in the first modal amplitude would correspond to simple harmonic motion in the first mode only. With the inclusion of the solar radiation disturbance (given by Eq. (23)) into the model, it is seen that the pitch motion is also excited. As an example, Fig. 3 illustrates the response of the beam to an initial displacement of $\varepsilon_1(0) = 0.01$ in the presence of the solar radiation disturbance where the fundamental flexural frequency is assumed to be ten times the orbital rate. The pitch motion also induces the dumbbell motion and oscillations in the second mode through coupling. The induced pitch amplitude is nearly 2^o.

The method adopted here to obtain control laws and the gain parameters for which an acceptable transient response would result in the presence of the disturbance is to first consider the control problem by ignoring the disturbance, D, in Eq. (22). The transient response of the system with the disturbance is obtained next, and then the gain parameters and, if necessary, also the form of the control laws will be modified to obain an acceptable system response under the action of the disturbances.

A set of gain parameters was obtained earlier by examining the characteristic equation of the dumbbell stabilized beam with one actuator at one end of the beam, for which the disturbances were completely ignored. The control law obtained was of the form

$$F_c = -0.07\theta - 0.005\dot{\varepsilon}_1 - 0.03\dot{\varepsilon}_2 \tag{25}$$

The transient responses with this control law for the dumbbell stabilized beam with and without the disturbances included in the system are shown in Fig. 4 for an initial displacement of 0.01ℓ in the first mode only. The fundamental frequency of the beam is assumed to be ten times the orbital frequency. The effect of the solar radiation disturbance is to increase the induced pitch amplitude slightly as shown in Fig. 4. The peak control force required is also increased by a small amount, but still is of the order of 10^{-4} Nt. only.

the control law for this case is seen to be acceptable under the expected solar radiation disturbance on the beam.

To study the robustness of this control system, an extreme case of the solar radiation disturbance is considered with an initial displacement of 0.1ℓ in the first mode for a beam whose fundamental frequency is 7 times the orbital frequency. For this case of the beam and based on the previous control law, Eq. (25), the transient response of the system is shown in Fig. 5 with and without the solar radiation disturbance. It is clearly seen that the dumbbell stabilized beam whose pitch motion is well controlled in the absence of the solar radiation disturbance, experiences extremely large amplitudes of pitch oscillations ($\pm 15^{o}$) due to the solar radiation disturbance. The transient performance of the system in all modes is improved simply by increasing the gain value corresponding to the modal rate by ten times and also the gain proportional to the pitch angle from -0.07 to -0.3, (Fig. 6), for the same initial conditions and beam parameters as in Fig. 5. The large amplitudes in the pitch motion disappear as the first modal amplitude is quickly damped reducing the magnitude of the solar radiation disturbance. The peak control force now increases by two orders of magnitude as compared with the cases in Fig. 3 and Fig. 4, but the peak force value of 2×10^{-2}Nt. is still a small value. Thus, the need to consider the solar radiation disturbance in designing a control system for a highly flexible system is demonstrated.

Control of a Flexible Beam Nominally Oriented Along the Local Vertical

The same procedure used for the dumbbell stabilized beam is repeated here to obtain a robust control law and the gain parameters for use with the solar disturbance input. The control law, with the gain parameters selected to provide damping in pitch and the first mode is given by

$$F_c = -0.01\,\dot{\theta} - 0.01\,\dot{\varepsilon}_1 \qquad (26)$$

The second mode is not included in this model, because the second mode is decoupled from pitch and the first mode, even in the presence of the solar radiation disturbance.[2] The system transient response with the solar radiation disturbance is shown in Fig. 7 for $\varepsilon_1(0) = 0.01\ell$ and the fundamental frequency of the beam assumed to be ten times the orbital frequency, and with and without the application of control. In the absence of control, the magnitude of the induced pitch oscillations ($\simeq 0.25^{o}$) is small as compared with the case of the dumbbell stabilized beam (Fig. 3), because of the stabilizing gravity forces. With the application of the control, damping in both pitch and the modal amplitude results

The same control law, (Eq. 26), applied to a more flexible beam ($\omega_1 = 3.0$) and a larger initial amplitude in the first mode ($\varepsilon_1(0) = 0.1\ell$) shows (Fig. 8) that the pitch amplitude overshoot is nearly 30^{o}. An attempt was made to increase the feedback gain proportional to the first flexible mode, ε_1, as before, for the case

of the dumbbell stabilized beam. The transient responses (not shown) indicated large overshoots in the pitch amplitude and a further increase in the feedback gain value made the system unstable. Similar attempts of varying the gain values corresponding to the pitch rate and providing the feedback proportional to the pitch angle failed to provide an acceptable transient response of the system. Two actuators were then assumed, one at the center of the beam (providing control over the flexible mode only) and the other at one of the nodal point ($\frac{x}{\ell} = 0.776$) of the flexible mode to control the pitch motion only. The pitch and the flexible mode were then decoupled except for the influence of the flexible mode on the pitch motion through the solar radiation disturbance. The following control laws were selected for the two actuators to provide critical damping in both pitch and the flexible mode.

$$f_1 = -0.113\dot{\theta} \qquad f_2 = -0.3\dot{\varepsilon}_1 \tag{27}$$

The transient response for the same initial conditions in Fig. 8 and under the new control law [Eq. (27)] is shown in Fig. 9. The pitch motion and the flexible modal oscillations are quickly damped out. The peak control force required is of the order of 10^{-2}Nt. for both the actuators - the same order of magnitude required in Fig. 8.

CONCLUSIONS

The uncontrolled and controlled dynamics of a thin flexible beam in orbit and in the presence of solar radiation disturbances are analyzed. Control laws and gain parameters are obtained to control: (i) the beam nominally oriented along the local horizontal and carrying a gimballed rigid dumbbell for gravity stabilization, and (ii) the beam nominally oriented along the local vertical. The control laws previously developed ignoring the environmental effects are found to be inadequate to control the shape and orientation of very flexible beams that are exposed to solar radiation disturbances. In order to obtain a robust control system in the presence of enviromental perturbations, it is sometimes more desirable to increase the number of actuators rather than simply modifying selected gain values. For further research related to the problem of minimizing the overshoot under large disturbances (in a qualitative manner) the use of pole placement techniques and application of linear quadratic Gaussian method are suggested as a follow on effort, especially for large order systems.

ACKNOWLEDGEMENT

This research was supported by NASA Grant NSG-1414, Suppl. 5,
Mr. H.A. Hamer, NASA-Langley, Technical Monitor.

REFERENCES

1. A.A. Karymov, "Determination of Forces and Moments Due to Light Pressure Acting on a Body in Motion in Cosmic Space," P.M.M., No. 5, Vol. 26, 1962, pp. 867-876.

2. R. Krishna and P.M. Bainum, "Effect of Solar Radiation Disturbance on a Flexible Beam in Orbit," AIAA 21st Aerospace Sciences Meeting, Reno, Jan. 10-13, 1983, Paper No. 83-0431.

3. P.M. Bainum and V.K. Kumar, "On the Dynamics of Large Orbiting Flexible Beams and Platforms Oriented Along the Local Horizontal," Acta Astronautica, Vol. 9, No. 3, 1982, pp. 119-127.

4. P.M. Bainum, R. Krishna and V.K. Kumar, "The Dynamics of Large Flexible Earth Pointing Structures with a Hybrid Control System," The Journal of the Astronautical Sciences, Vol. XXX, No. 3, July-September, 1982, pp. 251-267.

5. V.K. Kumar and P.M. Bainum, "Dynamics of a Flexible Body in Orbit," Journal of Guidance and Control, Vol. 3, No. 1, Jan.-Feb. 1980, pp. 90-92.

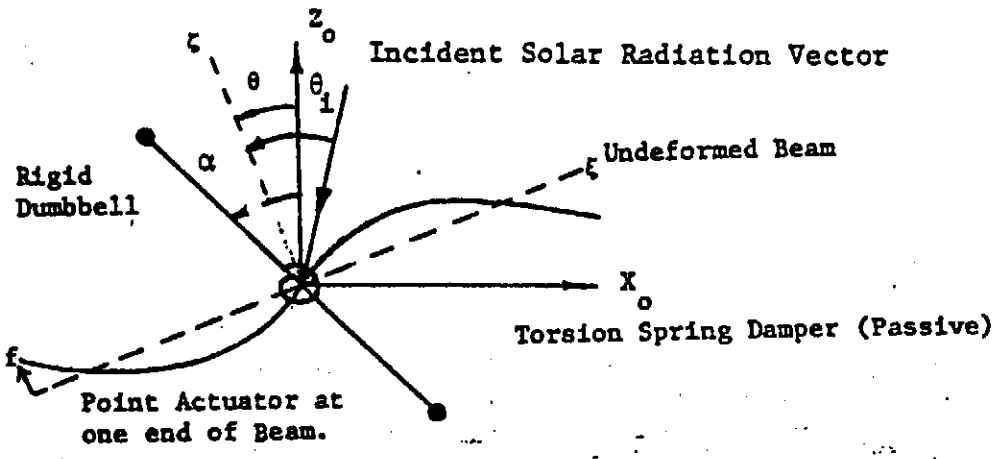

Fig. 1(a) Dumbbell Stabilized Flexible Beam Nominally Oriented along the Local Horizontal.

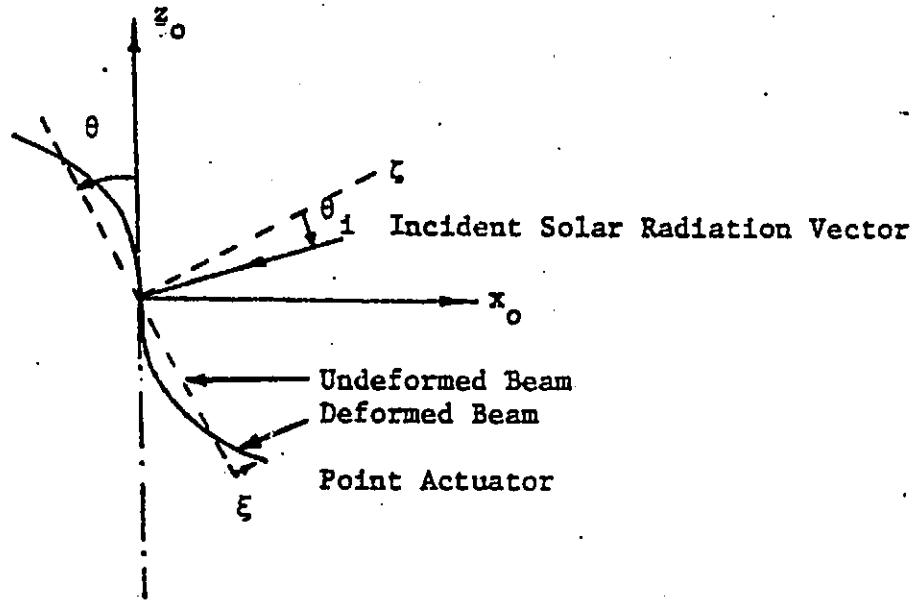

Fig. 1(b) Uniform Flexible Beam Nominally Oriented along the Local Vertical.

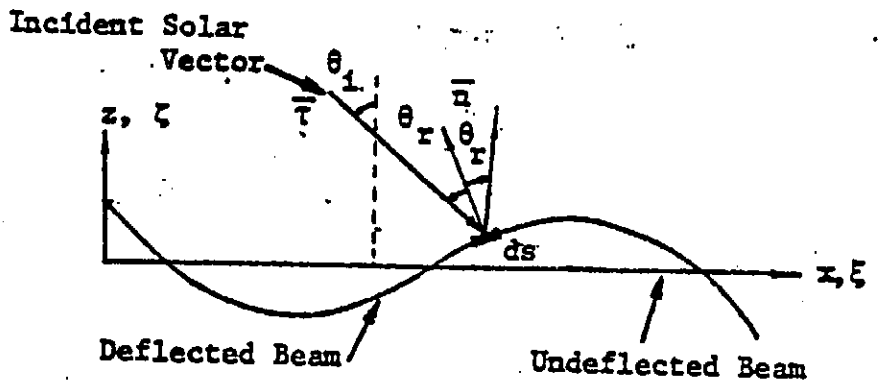

Fig. 2. Geometry of Raflection of a Flexible Beam Exposed to Solar Radiation.

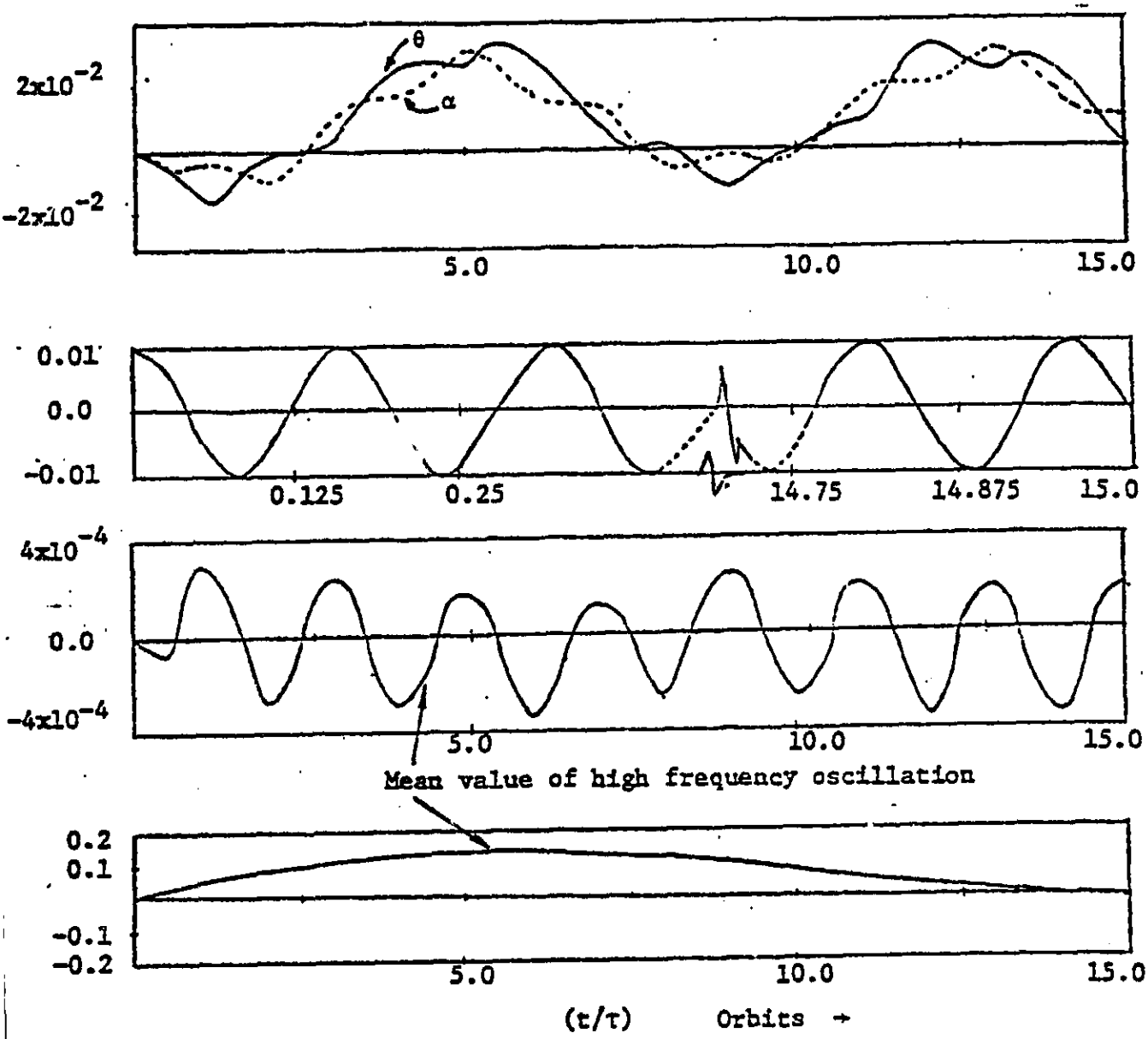

Fig. 3. Time Response of Dumbbell Stabilized Flexible Beam in the Presence of Solar Radiation Pressure. (ω_1 = 10.0).

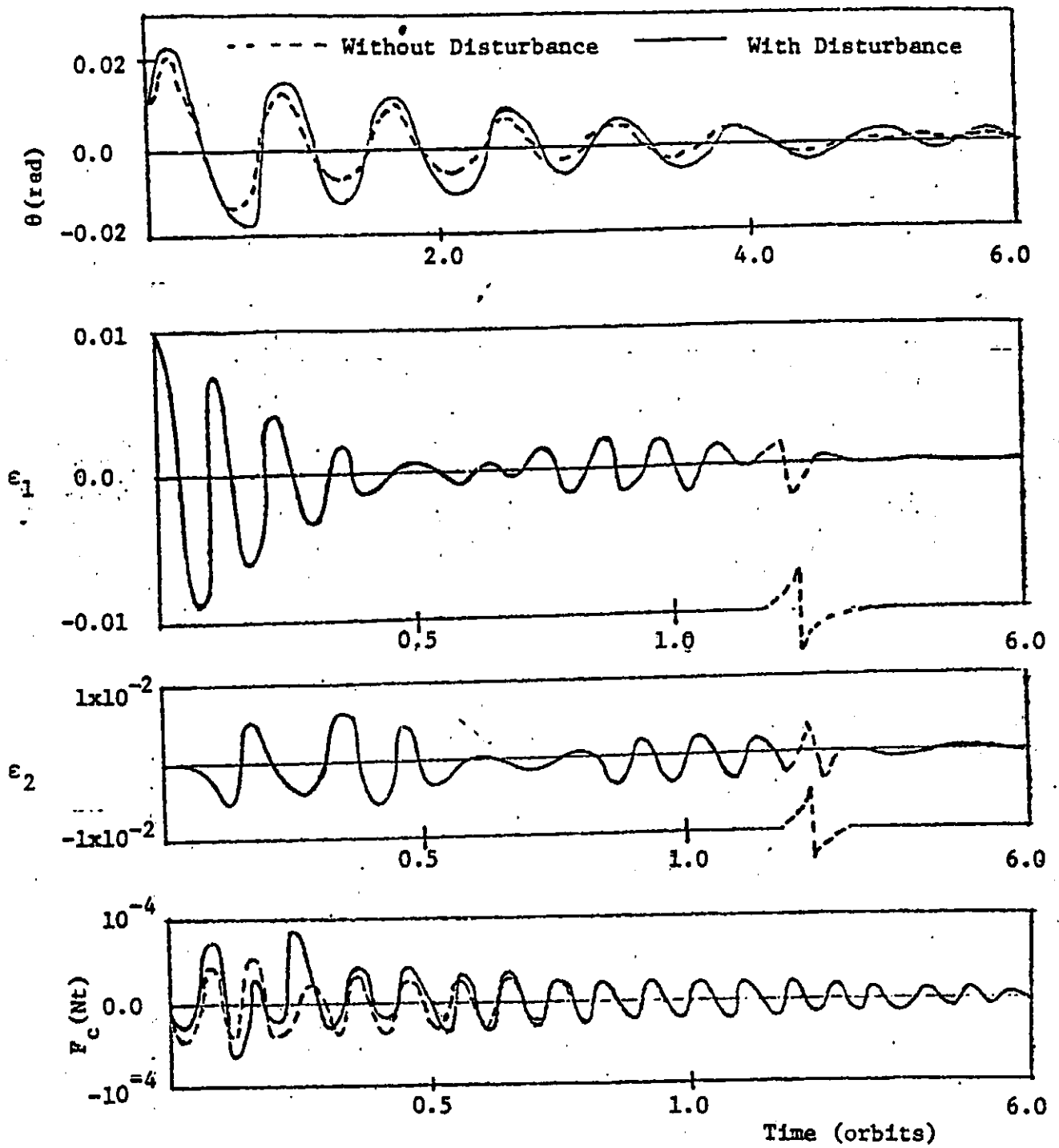

I.C.'S $\varepsilon_1(0) = 0.01, \quad \theta(0) = \alpha(0) = 0.0$

$F_c = -0.07\theta - 0.005\dot{\varepsilon}_1 - 0.03\dot{\varepsilon}_2 \quad \omega_1 = 10.0$

Fig. 4. Time Response of Dumbbell Stabilized Flexible Beam with Active Control - With and Without Solar Radiation Disturbance. (No Noticeable Change in the Presence of Solar Radiation Disturbance in ε_1 and ε_2.)

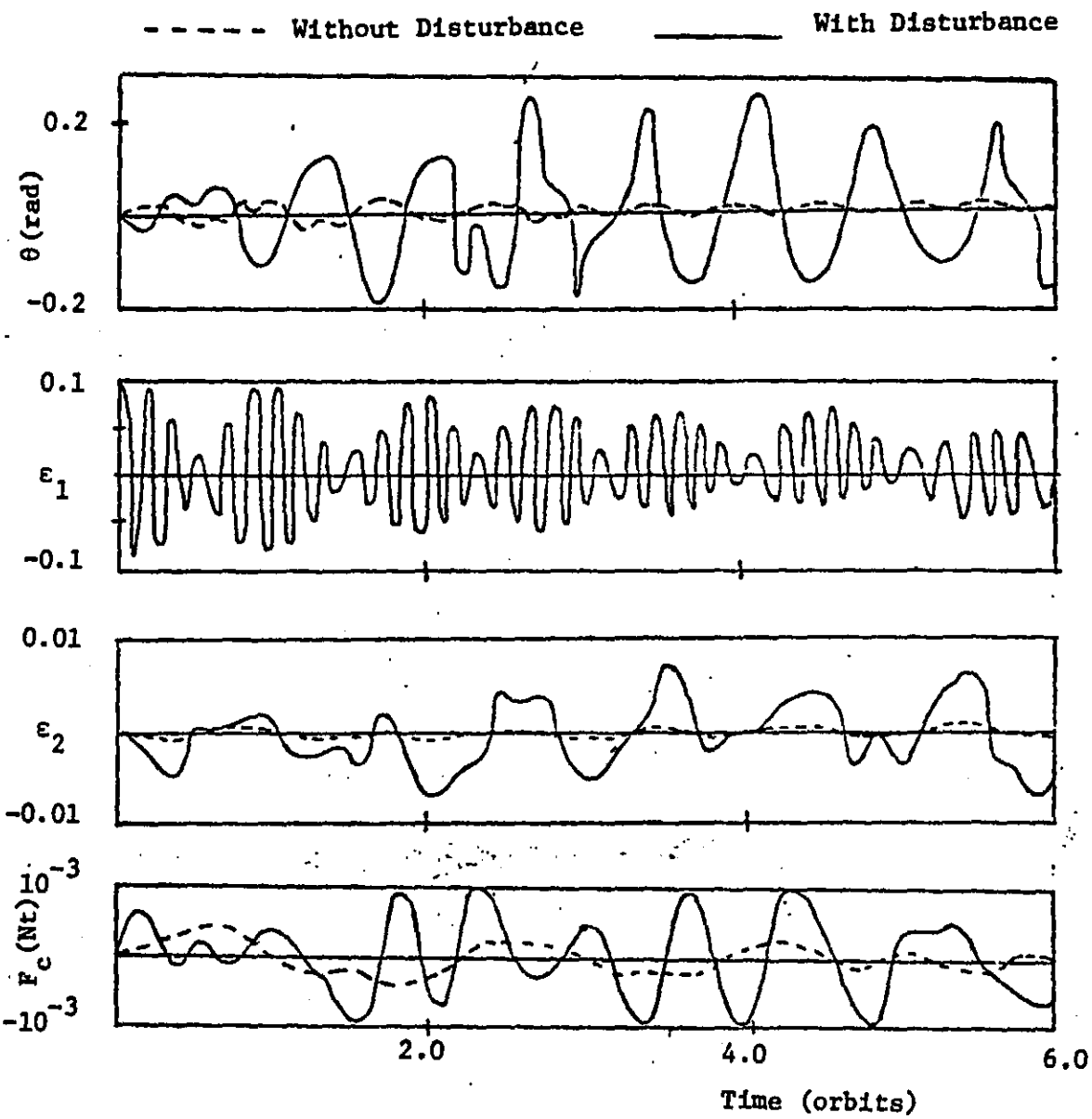

I.C.'s: $\varepsilon_1(0) = \dot{0}.1 \quad \theta(0) = \alpha(0) = \varepsilon_2(0) = 0.0$

$F_c = -0.07\theta - 0.005\dot{\varepsilon}_1 - 0.03\dot{\varepsilon}_2 \qquad \omega_1 = 7.0$

Fig. 5. Time Response of Dumbbell Stabilized Flexible Beam in Orbit with Active Control - With and Without Solar Radiation Disturbance.

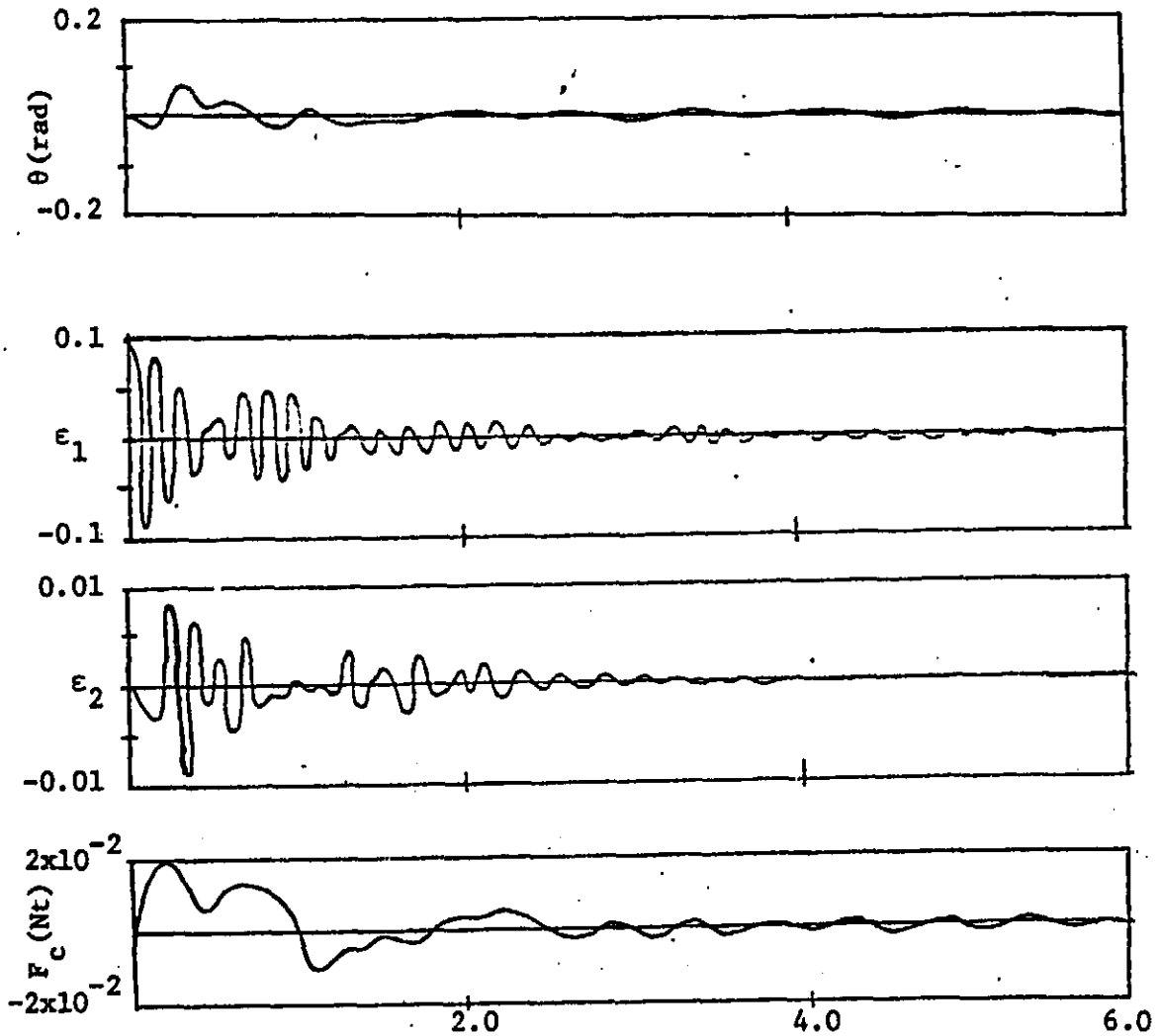

I.C.'s: $\varepsilon_1(0) = 0.1 \quad \theta(0) = \alpha(0) = \varepsilon_2(0) = 0.0$

$F_c = -0.3\theta - 0.05\dot{\varepsilon}_1 - 0.03\dot{\varepsilon}_2 \qquad \omega_1 = 7.0$

Fig. 6. Time Response of Dumbbell Stabilized Flexible Beam in Orbit with Modified Active Control and in the Presence of Solar Radiation Disturbance.

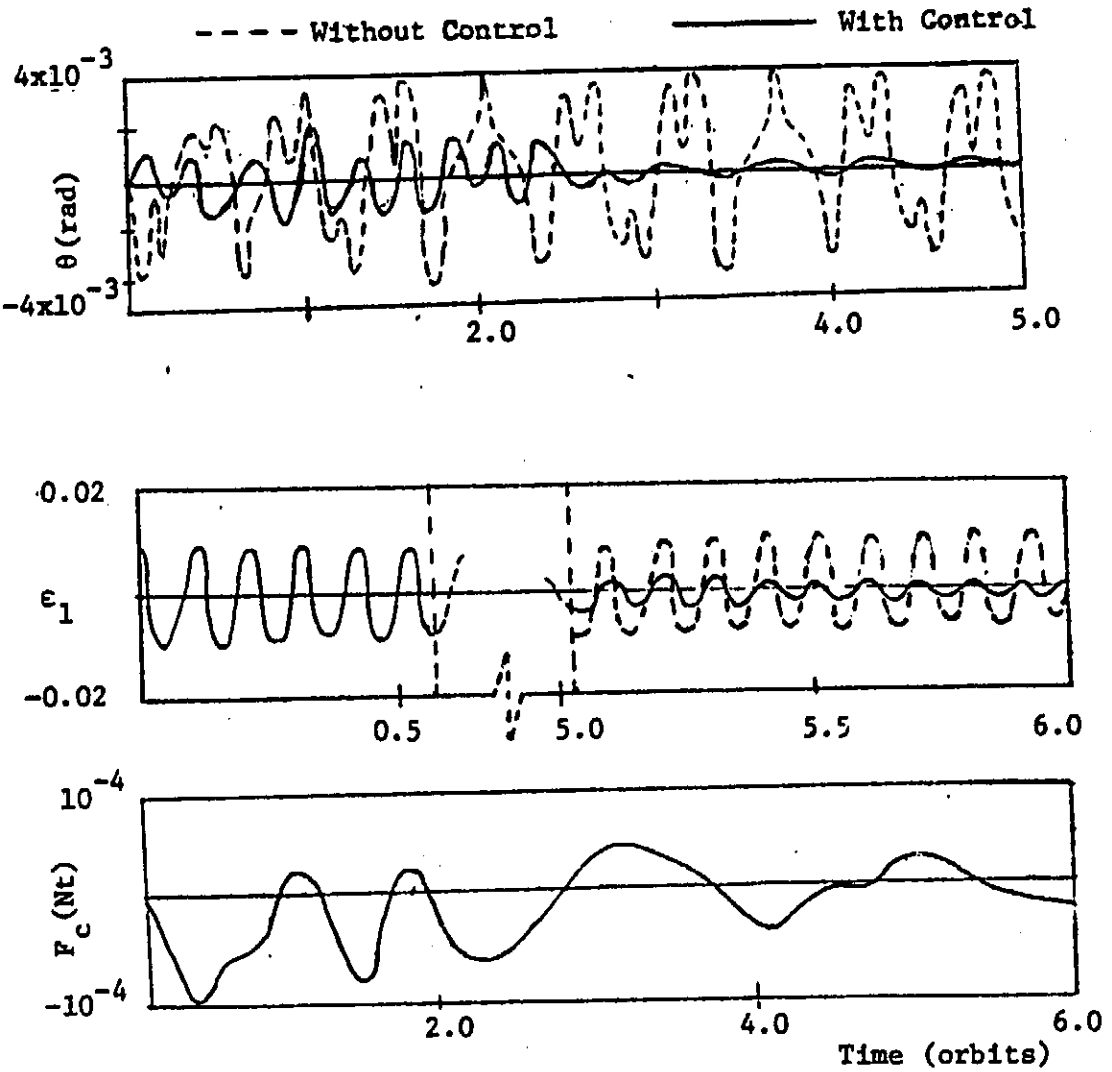

I.C.'s $\theta(0) = 0$ $\varepsilon_1(0) = 0.01$

$F_c = -0.01\,\dot{\theta} - 0.01\,\dot{\varepsilon}_1$ $\omega_1 = 10.0$

Fig. 7. Time Response of the Flexible Beam Nominally Oriented Along the Local Vertical and in the Presence of Solar Radiation Pressure.

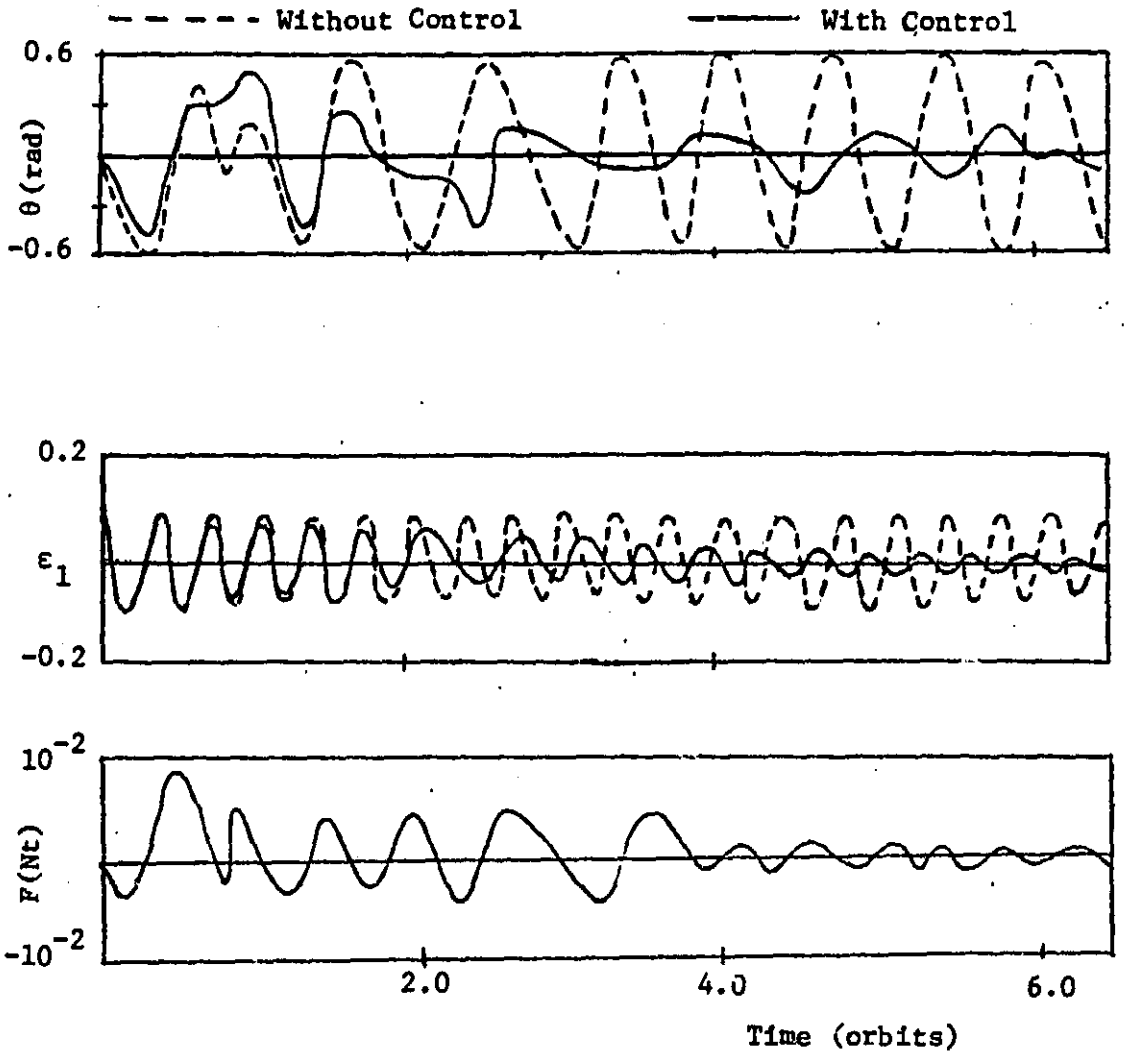

I.C.'s: $\varepsilon_1(0) = 0.1$ $\theta(0) = 0$ $\omega_1 = 3.0$

Fig. 8. Time Response of Flexible Beam Nominally Oriented Along the Local Vertical and in Presence of Solar Radiation Pressure and With and Without Active Control.

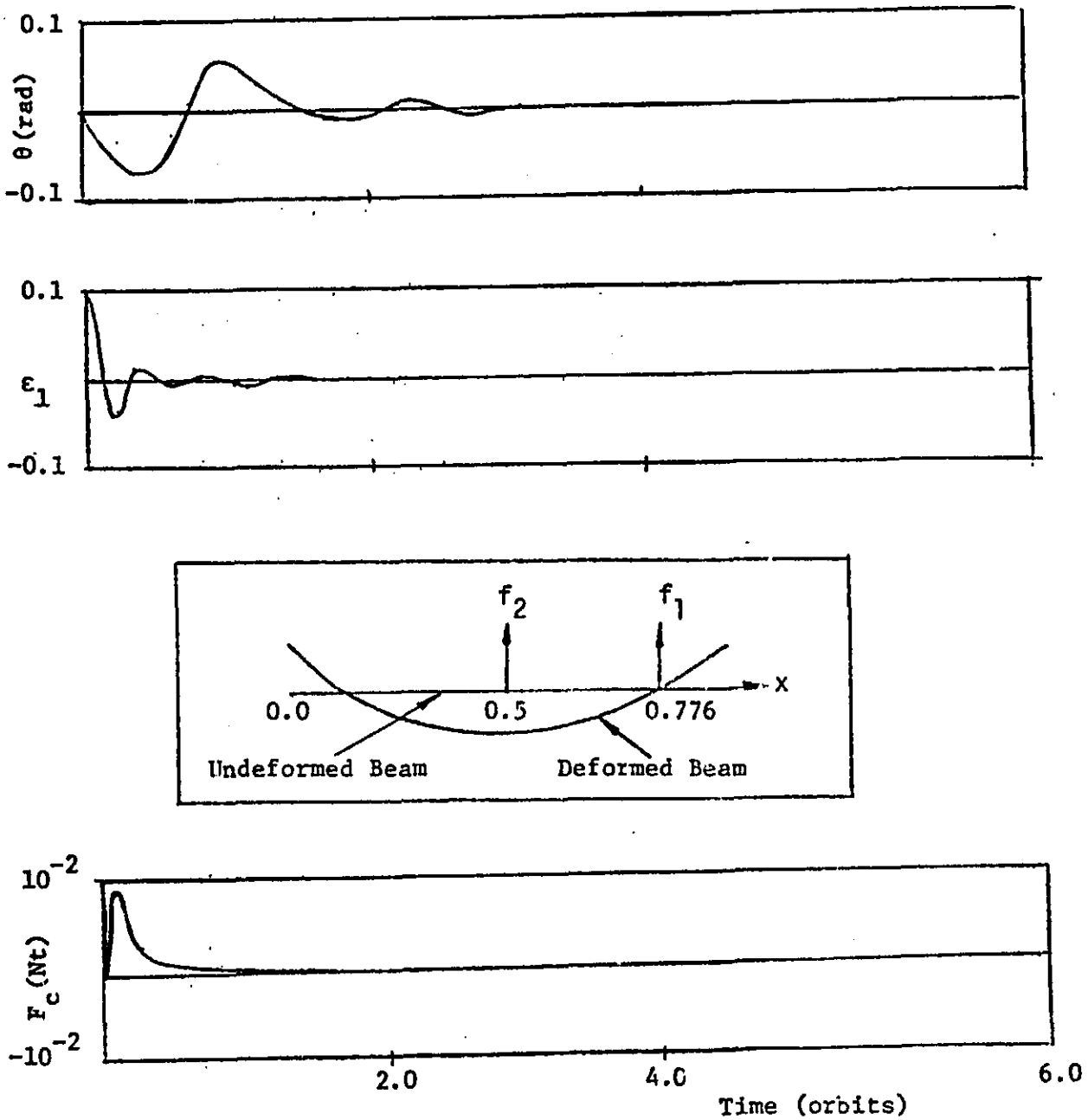

I.C.'s: $\theta(0) = 0$ $\quad \varepsilon_1(0) = 0.1$

$F_c = |\bar{f}_1| + |\bar{f}_2| \quad f_1 = -0.113\dot{\theta} \quad f_2 = -0.3\dot{\varepsilon}_1 \quad \omega_1 = 3.0$

Fig. 9. Time Response of Flexible Beam Nominally Oriented along the Local Vertical with Modified Active Control and in the Presence of the Solar Radiation Disturbance.

IV. EFFECT OF SOLAR RADIATION PRESSURE ON THE DYNAMICS OF A THIN HOMOGENEOUS SQUARE PLATE IN ORBIT

IV.1 Introduction

Proposed future applications of large space structures require control of the shape and orientation of the structure in orbit. It has been shown previously[1], considering a long, thin and uniform beam, that the principal environmental disturbance acting on these structures could be due to the solar radiation pressure. In the present work the dynamics of a more important basic structure, namely, a thin, homogeneous and flexible square plate exposed to solar radiation disturbance will be considered. The force and moment expressions as given by Karymov[2] will be used to obtain the expressions for solar radiation disturbing forces and moments acting on the free-free square plate in orbit. The dynamics of such a plate nominally oriented along the local vertical was considered earlier disregarding the environmental disturbances.[3] In the present study it is proposed to reconsider the dynamics of the square plate nominally oriented along the local vertical with the solar radiation force and moment expressions included in the dynamic model.

The mode shapes and the frequencies of the plate are obtained using the finite element program, STRUDL.[4] To obtain expressions for solar radiation forces and moments, it is convenient to express the mode shapes of the plate as a combination of the mode shapes of a free-free beam.[5] The first five modes of the plate will be considered for study here. The plate is assumed to have only small transverse vibrations, so that the shadowing of the plate due to any deflected part of the plate can be neglected. The small deflection assumption also allows the superposition of the beam mode shapes in representing the mode shapes of the plate.

IV.2 Solar Radiation Forces and Moments Acting on a Thin Homogeneous Flexible Square Plate

Fig. 4.1 shows a square plate exposed to solar radiation. Let $\bar{n}$ denote the outward unit vector normal to the surface, ds. and let $\bar{\tau}$ be the unit vector in the direction of solar radiation denoted as

$$\bar{\tau} = a_o \bar{i} + b_o \bar{j} + c_o \bar{k} \tag{4.1}$$

The direction cosines of $\bar{\tau}$, namely, a_o, b_o and c_o, can be expressed in terms of the solar incidence angles, θ_i and ψ_i, (defined in Fig. 4.1) as

$$\begin{aligned} a_o &= \sin\theta_i \cos\psi_i \\ b_o &= \sin\theta_i \sin\psi_i \\ c_o &= \cos\theta_i \end{aligned} \tag{4.2}$$

Then, the solar radiation force, $\bar{F}_a$, and the moment, $\bar{N}_a$, on a completely absorbing surface are given by[2]

$$\bar{F} = h_o \bar{\tau} \int_s \bar{\tau}\cdot\bar{n}\, ds \tag{4.3}$$

and

$$\bar{N}_a = -h_o \bar{\tau} \times \int_s \bar{R}\,(\bar{\tau}\cdot\bar{n})\, ds \tag{4.4}$$

where, $h_o = 4.64\times10^{-6}$ Nt/m^2 is a constant for near earth space structures. The integration over the area, s, is bounded by the condition

$$\bar{\tau}\cdot\bar{n} \geq 0 \tag{4.5}$$

The force, $\bar{F}_r$, and moment, $\bar{N}_r$ acting on a completely reflecting surface can be developed as[2],

$$\bar{F}_r = -2h_o \int_s \bar{n}\,(\bar{\tau}\cdot\bar{n})^2\, ds \tag{4.6}$$

and

$$\bar{N}_r = 2h_o \int_s \bar{n}\times\bar{r}\,(\bar{\tau}\cdot\bar{n})^2\, ds \tag{4.7}$$

where, $\bar{R}$ is the position vector of ds with respect to the center of mass of the plate.

For a surface with an arbitrary reflection coefficient, ϵ_r, the force and moment expressions become[2]:

$$\bar{F}_{\epsilon r} = \bar{F}_a + \epsilon_r(\bar{F}_r - \bar{F}_a)$$
$$\bar{N}_{\epsilon r} = \bar{N}_a + \epsilon_r(\bar{N}_r - \bar{N}_a) \tag{4.8}$$

The shape function of a rectangular plate can be represented as a product of the two beam functions given by[5] (considering only the transverse vibration),

$$Z_{m,n}(x,y) = \theta_n(x)\,\psi_m(y) \tag{4.9}$$

θ and ψ are the free-free beam shape functions given by

$$\theta_n(x) = \sigma_n(\sin\Omega_n x + \sinh\Omega_n x) + (\cos\Omega_n x + \cosh\Omega_n x)$$
$$\text{for } n = 2,3,4 \ldots . \tag{4.10}$$

where, $\sigma_n = (\cos\Omega_n - \cosh\Omega_n)/(\sinh\Omega_n - \sin\Omega_n)$

and $\theta_n(x) = 1-2x$ for $n=1$

$= a$ constant for $n=0$

and $\theta_n(x) \equiv \psi_n(y)$

For a square plate, certain special modes which are combinations of the modes of a rectangular plate are shown to be existing.[5] The frequency expressions for such modes are also given in Ref. 5. The first five modes of a square plate in which the second and third modes represent special combinations of "beam modes" (Fig. 4.2) are considered in the present study.

A unit normal to the syrface, $\bar{n}$, is given by,

$$\bar{n} = a_1\bar{i} + b_1\bar{j} + c_1\bar{k}$$

$$= \frac{\psi(d\theta/d\xi)\bar{i} + \theta(d\psi/d\eta)\bar{j} - \bar{k}}{\sqrt{(\psi\, d\theta/d\xi)^2 + \theta\,(d\psi/d\eta)^2 + 1}} \qquad (4.11)$$

(ξ, η, ζ) are non-dimensional coordinates in the x,y,z directions, respectively.) The position vector, $\bar{R}$, is represented as,

$$\bar{R} = (\xi - \tfrac{1}{2})\,\bar{i} + (\eta - \tfrac{1}{2})\,\bar{j} + z\,\bar{k} \qquad (4.12)$$

Eqs. (4.1), (4.11) and (4.12) are substituted into Eq. (4.4) and then the resulting integrals are evaluated to obtain the expression for the moment acting on a plate having a completely absorbing surface as,

$$\bar{N}_a = -h_o\ell^2[\{b_o s_3 - c_o(s_2 - s_4/2)\}\,\bar{i} + \{c_o(s_1 - s_4/2) - a_o s_3\}\,\bar{j} + \{a_o(s_2 - s_4/2) - b_o\,(s_1 - s_4/2)\}\,\bar{k}] \qquad (4.13)$$

where,

$$s_1 = \int_s \xi s_c\, d\xi d\eta \qquad s_2 = \int_s \eta s_c\, d\xi d\eta$$

$$s_3 = \int_s \zeta s_c\, d\xi d\eta \qquad s_4 = \int s_c\, d\xi d\eta$$

$$s_c = \left(a_o\psi_m \frac{d\theta_n}{d\xi} + b_o\,\theta_n \frac{d\psi_m}{d\eta} - c_o\right)$$

The integrals s_1 to s_4 can be evaluated analytically. The moment expressions are obtained for the first five plate modes (Fig. 4.2) by evaluating s_1 to s_4 for combinations of corresponding (m,n) modes and are given as,

$$\bar{N}_a = \frac{h_o\ell^2}{3}\,[a_o c_o\bar{i} - b_o c_o\bar{j} + (b_o^2 - a_o^2)\bar{k}]\, z_1 \quad \text{(for mode I)}$$

$$= h_o\ell^2 c_o\,[b_o\bar{i} + a_o\bar{j}]\, z_2 \quad \text{(for mode II)}$$

$$= h_o\ell^2 c_o\,[b_o\bar{i} - a_o\bar{j}]\, z_3 \quad \text{(for mode III)}$$

$$= o, \quad \text{(for modes IV and V)} \qquad (4.14)$$

where, z_1, z_2 and z_3 are deflections at one corner of the plate associated with the I, II and III modes, respectively.

The moment due to solar radiation pressure, $\bar{N}_r$, acting on a completely reflecting surface is obtained by substituting Eqs. (4.11), (4.12) and (4.1) in Eq. (4.7). The resulting integral is simplified to obtain the expression,

$$\bar{N}_r = 2h_o \int_s [(a_2\zeta - a_3\eta')\bar{i} + (a_3\xi' - a_1\zeta)\bar{j} + (a_1\eta' - a_2\xi')\bar{k}]\, s_c\, d\xi d\eta \qquad (4.15)$$

where, $\xi' = \xi - 0.5$ and $\eta' = \eta - 0.5$

Eq. (4.15) involves complicated integrals and to find an analytical solution is very difficult. Instead, a numerical evaluation of the integrals involving different modes are carried out and the results are shown in Fig. 4.3. The plate dimension is considered to be 100mx100m and the deflection at the corner of the plate for each mode is assumed to be $z_1 = z_2 = z_3 = 1.0$m. Similar results are also shown in Fig. 4.3 for a plate having a completely absorbing surface and are obtained using Eq. (4.14). The solar incidence angle, θ_i, is varied from 0 to 90^o, with $\psi_i = 0$. Only the first three modes give rise to appreciable moments for both completely absorbing and completely reflecting surfaces. The magnitudes of the moments are seen to be an order of magnitude higher (2×10^{-2} Nt-m) for a completely absorbing surface as compared with the case of a completely reflecting surface (10^{-3} Nt-m). The moments due to modes II and III, and for both completely reflecting and completely absorbing surfaces, can be visualized as extensions of the result obtained for the case of the beam.[1] For $\psi_i = 0^o$ (incidence only in the z,x plane) the moment on a beam is shown to be about the y axis for any given mode of the beam.

But, for the same case, interaction of the solar pressure on the plate vibrating in only the first mode, results in a moment about the x-axis. The reason for the latter phenomena can be explained by considering the force distribution for a completely absorbing surface (Fig. 4.4). There is a finite moment about the x-axis along the cross section y'-y' as shown in Fig. 4.4 because of the uniform variation in the angle of incidence along y'-y'. All the cross sections must be similarly considered from $\xi = 0$ to 1, and the net moment result will, in general, be non zero. A similar explanation can be given for the case of a completely reflecting surface.

Based on the numerical results shown in Fig. 4.3, in which ψ_1 is varied from 0 to 90° (not shown) the moment expressions for a completely reflecting plate can be written as,

$$\begin{aligned}\bar{N}_r &= h_1 c_o (a_o\bar{i} - b_o\bar{j})\, z_1 \quad \text{(for mode I)} \\ &= h_2 c_o (b_o\bar{i} - a_o\bar{j})\, z_2 \quad \text{(for mode II)} \\ &= h_2 c_o (b_o\bar{i} - a_o\bar{j})\, z_3 \quad \text{(for mode III)}\end{aligned}$$

where, $h_1 = 3.25\times10^{-4}$ and $h_2 = 1.09\times10^{-3}$

Eq. (4.16) is found to be valid for magnitudes of z_1 to z_3 up to 0.01ℓ. The moments about the x,y and z axes are obtained by collecting the coefficients of $\bar{i}$, $\bar{j}$ and $\bar{k}$, respectively, from Eqs. (4.14) and (4.16) as,

$$\begin{aligned}N_{ax} &= h_3 \{(a_o/3)z_1 + b_o(z_2+z_3)\} \\ N_{ay} &= -h_3 \{(b_o/3)z_1 + b_o(z_3-z_2)\} \\ N_{az} &= (h_3/3)(b_o^2 - a_o^2)z_1\end{aligned} \qquad (4.17)$$

where $h_3 = h_o \ell^2 c_o$

$$N_{rx} = c_o\{h_1 a_o z_1 + h_2 b_o (z_2 - z_3)\}$$
$$N_{ry} = -c_o\{h_1 b_o z_1 + h_2 a_o (z_2 - z_3)\} \qquad (4.18)$$
$$N_{rz} = 0$$

Eqs. (4.17) and (4.18) are now substituted into Eq. (4.8) to obtain the moment acting on a plate with a surface of general coefficient of reflectivity, ε_r.

IV.3 Modal Forces Due to Solar Radiation Pressure

The effect of the disturbance on the generic mode is obtained by evaluating the integral[6]

$$E_n = \int z\ (x,y)\ \bar{k}\cdot d\bar{F} \tag{4.19}$$

where, $\bar{F}$ represents the force due to solar radiation pressure. Also,

$$E_n = E_{na} + \varepsilon_r\ (E_{nr}-E_{na}) \tag{4.20}$$

Eq. (4.3) is substituted into Eq. (4.19) and after evaluating the resulting integrals, E_{na} is found to be equal to zero for all modes of the plate. Eq. (4.6) is used in Eq. (4.19) to get

$$E_{nr} = 2h_o \int [z(a_o a_1+b_o b_1+c_o)/(a_1^2+b_1^2+1)]\ d\xi d\eta \tag{4.21}$$

The slopes, $d\theta_n/d\xi$ and $d\psi_n/d\eta$, are assumed to be very small so that $a_1^2+b_1^2+c_1^2 \simeq 1$. Thus, the integral in Eq. (4.21) can be easily evaluated to show that E_{nr} is also equal to zero for all modes of the plate. Hence, the solar radiation pressure does not give rise to any generic force. The results obtained can now be used in the dynamic model of a flexible plate in the orbit.

IV.4 Effect of Solar Radiation Pressure on a Plate Nominally Oriented Along the Local Vertical

The major surface of the plate is assumed to be perpendicular to the orbital plane (Fig. 4.5). From the general formulation of Refs. 3 and 5, the equations of motion of the structure are obtained, under the assumption that the transverse deformations are small compared to the characteristic length of the plate. The linearized equations of motion are given by[3]

$$\begin{aligned}
\ddot{\psi} &= -2\omega_c\dot{\phi} + \omega_c^2\psi + N_x/J_x \\
\ddot{\phi} &= \omega_c\dot{\psi} + N_y/J_y \\
\ddot{\theta} &= -3\omega_c^2\theta + N_z/J_z \\
\ddot{\epsilon}_n &+ (\Omega_n/\omega_c)^2\,\epsilon_n = 0
\end{aligned} \tag{22}$$

where ψ, ϕ, and θ refer to the yaw, roll, and pitch modes, respectively, ω_c is the orbital angular rate, Ω_n is the n^{th} modal frequency, ϵ_n is the non-dimensional modal amplitude, and $J_{x,y,z}$ are the principal plate moments of inertia.

The roll and yaw equations of motion are coupled to each other and the characteristic equation shows a double pole at the origin indicating instability in the roll-yaw motion. However, for an initial condition of $\psi(o) = \phi(o) = 0$, the roll and yaw motions will not build up. To study the effect of solar radiation disturbance, a square plate whose fundamental frequency is ten times the orbital frequency is considered. Only the first three flexible modes are included in the dynamic model with initial conditions of 0.01 in each mode. The transient response of the plate under the influence of solar radiation pressure is shown in Fig. 4.6.

The torque about the normal to the plate due to the first modal amplitude acts in one direction only (Fig. 4.3b); as the solar incidence angle changes in the orbit, it is seen that the cyclic contribution due to N_{ax} averages to zero. This torque induces a steady drift in the roll angle ($\simeq 1.5^{o}$ in 6 orbits). The yaw motion is seen to be oscillating with a very small amplitude (0.3^{o}). The solar radiation pressure disturbance also induces a small amplitude (0.03^{o}) pitch oscillation. The modal oscillations are unaffected in the presence of the solar radiation disturbance. The magnitude of the pitch, roll and yaw angular motions due to the solar radiation pressure are small becuase of the stabilizing gravity-gradient forces acting on the plate.

References - CHAPTER IV

1. Krishna, R. and Bainum, P.M., "Effect of Solar Radiation Disturbance on a Flexible Beam in Orbit," AIAA 21st Aerospace Sciences Meeting, Reno, Jan. 10-13, 1983. Paper No. 83-0431.

2. Karymov, A.A., "Determination of Forces and Moments Due to Light Pressure Acting on a Body in Motion in Cosmic Space," P.M.M., No. 5, Vol. 26, 1962, pp. 867-876.

3. Reddy, A.S.S.R., Bainum, P.M., Krishna, R., and Hamer, H.A., "Control of a Large Flexible Platform in Orbit," Journal of Guidance and Control, Vol. 4, No. 6, Nov.-Dec., 1981, pp. 642-649.

4. "ICES STRUDL II, the Structural Design Language," Massachusettes Institute of Technology, V2M2, 1972.

5. Warburton, G.B., "The Vibration of Rectangular Plates," Proceedings of the Institute of Mechanical Engineers, Vol. 168, No. 12, 1954, pp. 371-394.

6. Kumar, V.K., and Bainum, P.M., "Dynamics of a Flexible Body in Orbit," Journal of Guidance and Control, Jan.-Feb., 1980, Vol. 3, No. 1, pp. 90-92.

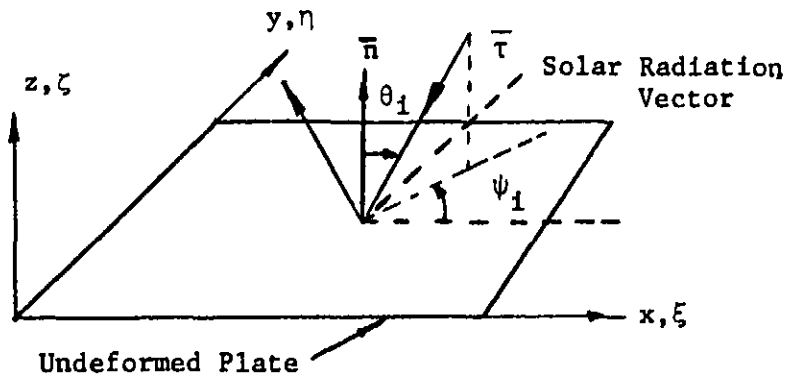

Fig. 4.1. A Thin Plate Exposed to Solar Radiation Pressure.

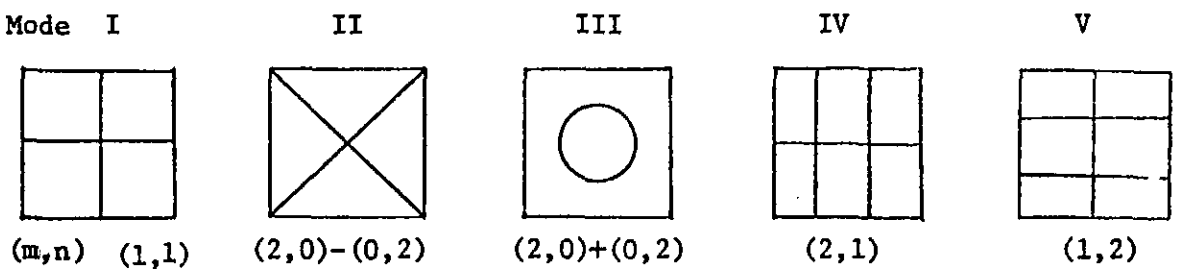

Fig. 4.2. The First Five Mode Shapes of a Square Plate.

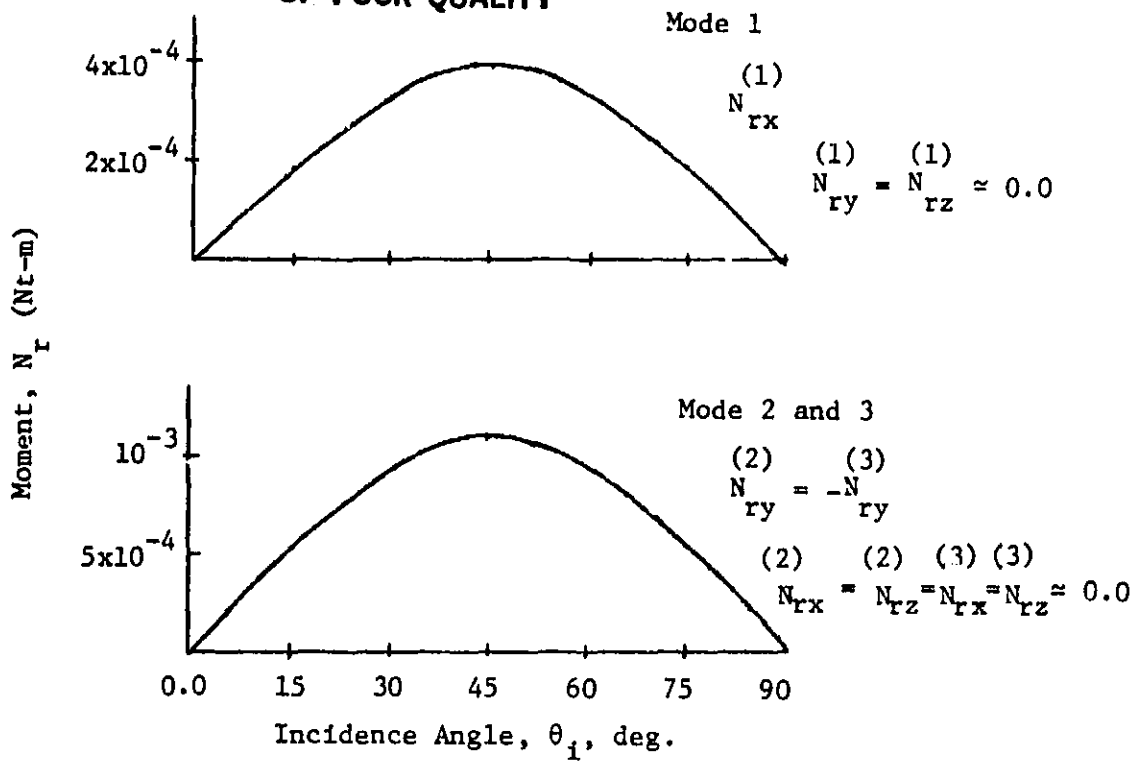

(a) Completely Reflecting Surface

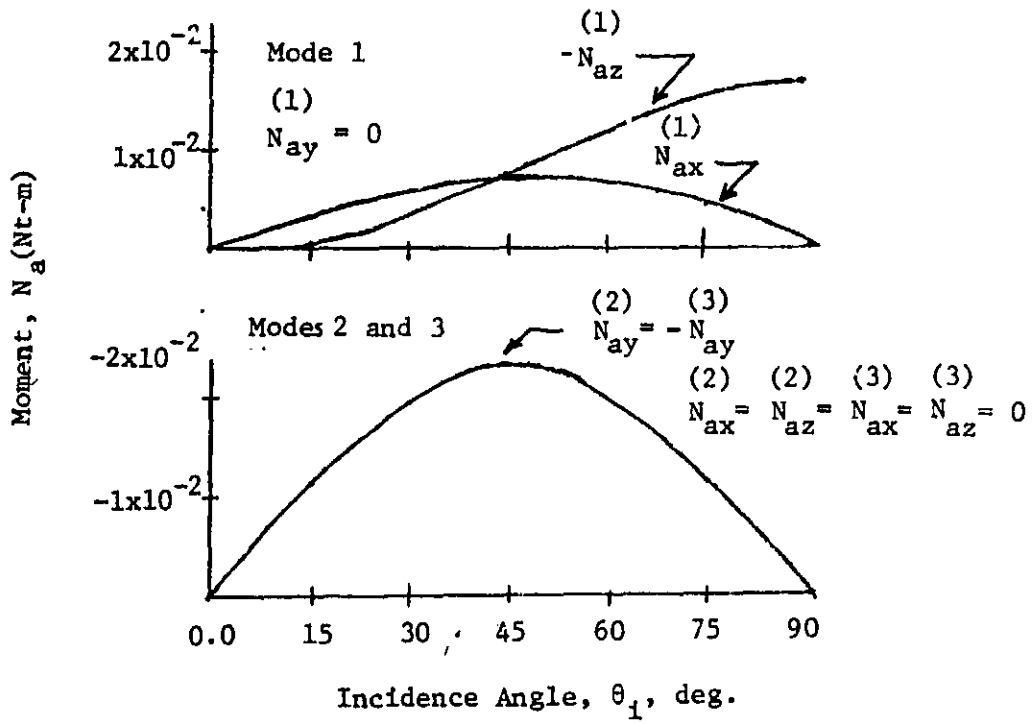

(b) Completely Absorbing Surface

Fig. 4.3 Moment due to Solar Radiation Pressure on a Plate ($\psi_i = 0.0$)

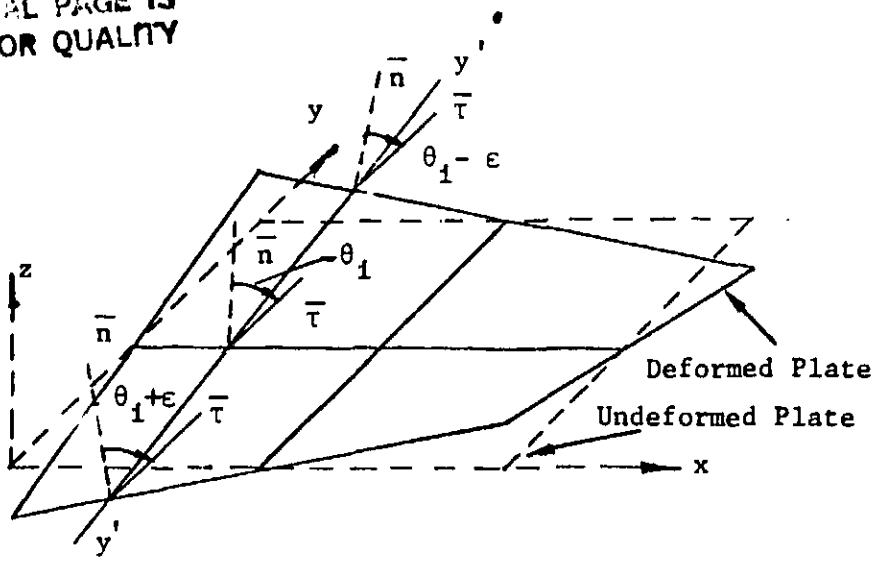

Fig. 4.4 Force Distribution due to the Interaction of Solar Pressure on a Completely Absorbing Plate Vibrating in the First Mode.

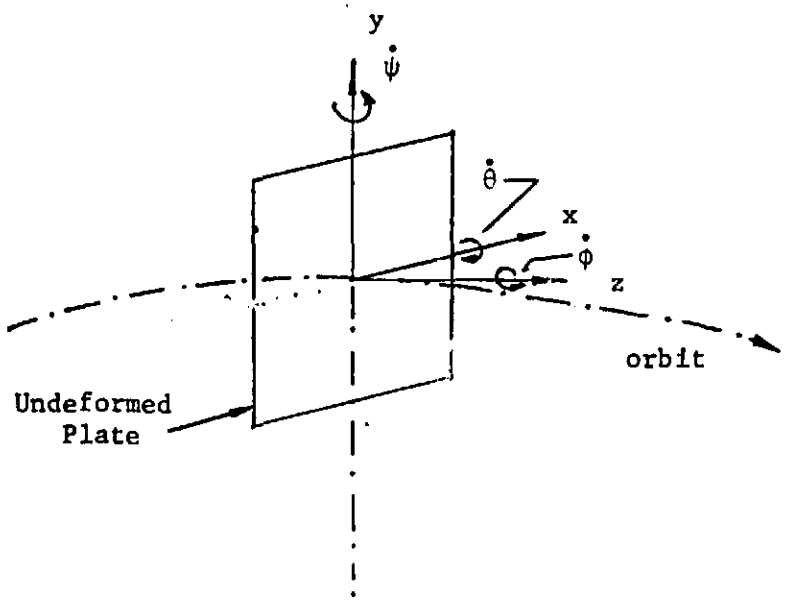

Fig. 4.5 A Square Plate in Orbit Nominally Along the Local Vertical.

I.C.'s $\psi(0) = \phi(0) = \theta(0) = 0$, $\varepsilon_1(0) = \varepsilon_2(0) = \varepsilon_3(0) = 0.01$

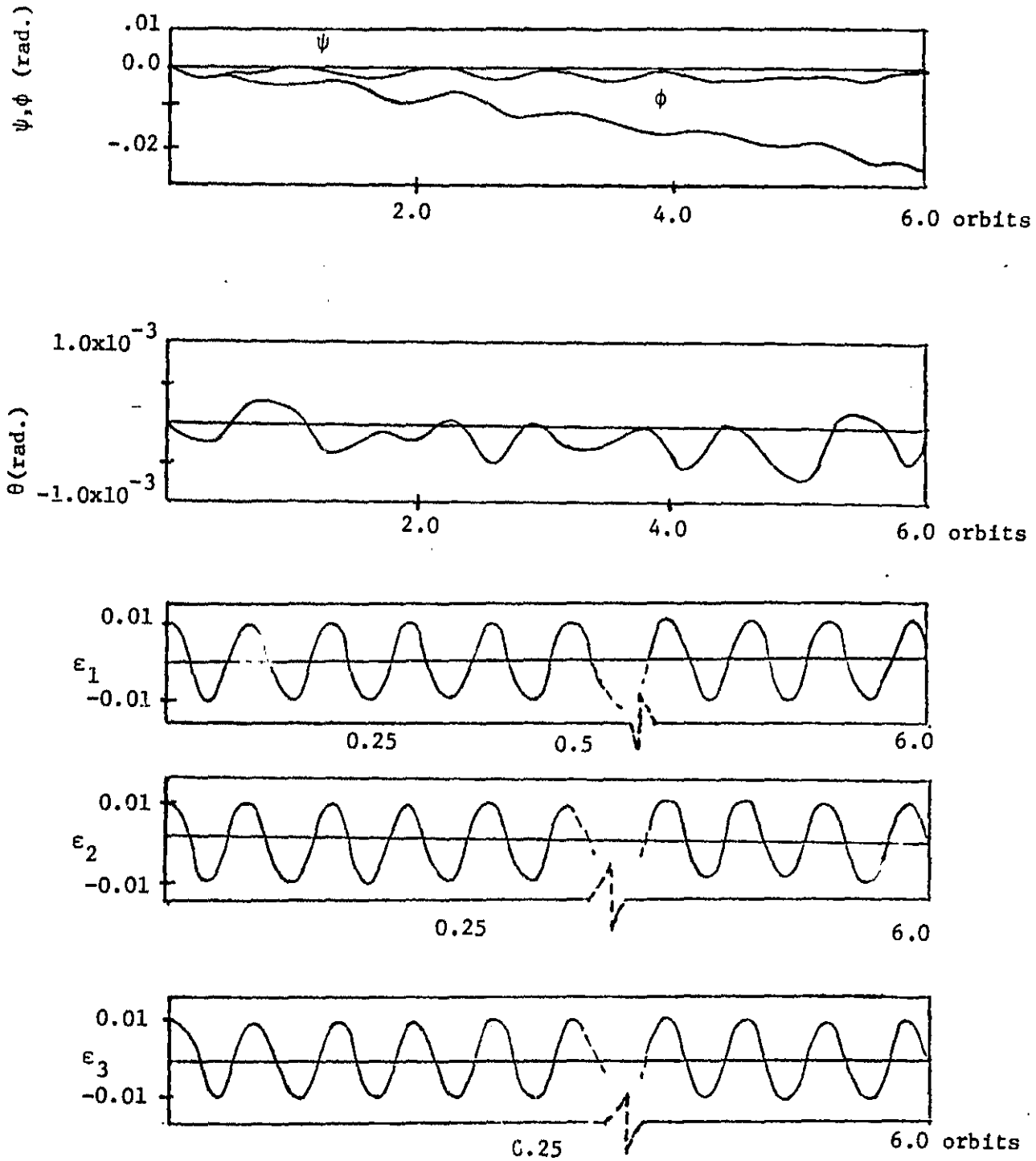

Fig. 4.6. Time Response of the Plate Nominally Oriented Along the Local Vertical Under the Influence of Solar Radiation Pressure.

V. SOLAR RADIATION HEATING EFFECTS ON THIN RECTANGULAR PLATES AND BEAMS

V.1 Introduction

The thermal gradients induced in large flexible space structures due to solar radiation heating can cause large deflections depending on the thermal properties of the material and the geometric shape of the structure. The thermal deflections are functions of both time and elastic displacements.[1,2] The heat being radiated from a thin solid is also proportional to the fourth power of the surface temperatures. Therefore, in order to study the effects of solar heating, a number of realistic assumptions, depending on the problem, will have to be made to obtain expressions for the important thermal effects.

The objective of the study here is to find expressions for thermal deflections of large, flexible, thin beams and plates exposed to solar heating. The major assumptions made here are: (a) the reflected solar radiation by the Earth (albedo) can be neglected; (b) the inherent time lags in the heat transfer process are very small compared with the orbital period; (c) the radiation from the edge surfaces can be neglected; and, (d) the beams and plates have uniform thickness and thermal properties resulting in a uniform temperature distribution of the surface facing the sun. The effects of the Earth's shadow and shadowing due to a part of the structure are not included in the study.

V.2 Equilibrium Temperatures of Thin Plates and Beams

The one dimensional beam bending analysis also applies to the two dimensional plate bending.[3] Fig. 5.1 shows the beam exposed to solar radiation. The solar incidence angle, θ_i, is taken to be a constant during a small interval of time. During this interval the surface facing the sun, s_u, attains temperature T_1 and the surface away from the sun, s_ℓ, attains a temperature, T_2. The equilibrium temperatures, T_1 and T_2, can be determined by writing the thermal balance equations. The total heat leaving the beam from the two surfaces, s_u and s_ℓ, should be equal to the heat received by the beam. Therefore,

$$E_1\sigma T_1^4 + E_2\sigma T_2^4 = \alpha_s G \cos\theta_i \tag{5.1}$$

where,

E_1 and E_2 are the emissivities of the surfaces, s_u and s_ℓ, respectively

σ = Stefan-Boltzman constant

= 56.7×10^{-12} KW/m^2 $^oK^4$

α_s = absorptivity of the surface, s_u

G = intensity of solar radiation $\simeq$ 0.8 KW/m^2

The heat flowing through the plate, at equilibrium, is also equal to the heat radiated from the surface, s_ℓ.

$$E_2\sigma T_2^4 = K(T_1-T_2)/t_c \tag{5.2}$$

where,

K = thermal conductivity (KW/m^{o}k) of the plate material

t_c = thickness of the plate

Equations (5.1) and (5.2) can be rearranged as

$$T_1 = T_2 + \frac{E_2\sigma t_c}{K} T_2^4 \tag{5.3}$$

$$T_2^4 = \frac{\alpha_s G \cos\theta_i}{E_2\sigma} - \frac{E_1}{E_2} T_2^4 \tag{5.4}$$

Eqs. (5.3) and (5.4) can now be solved to obtain T_1 and T_2 by assuming an approximate value of T_1 or T_2 and then through numerical iteration. Assuming $E_1 = E_2 = 0.05$ and $\alpha_s = 0.2$, the temperature difference, $\Delta T = T_1 - T_2$, is obtained as a function of the solar incidence angle, θ_i, and various parameter ratios of $k_r = k/t_c$, as shown in Fig. 5.2. A higher value of k_r indicates a larger value of thermal conductivity and, hence, the temperature difference between the two surfaces becomes smaller. A plate of thickness 1cm and made of Polyamide ($K = 0.25 \times 10^{-3} KW/m^{o}K$) will have a maximum temperature difference of $2.3^{o}K$. The temperature gradient is found to vary approximately linearly with θ_i from Fig. 5.2. Expressions for deflections of the plate as a function of the temperature gradient are developed, next.

V.3 Pure Bending of a Beam (or a Plate)[3]:

Fig. 5.3 shows a beam of length, ℓ, and width, b. The temperature of the mid-plane of the beam is denoted by T_n. The temperature of the surface facing the sun, s_u, is then $T_n+(\Delta T/2)$, and the temperature of the surface, s_ℓ, is given by $T_n-(\Delta T/2)$. According to the theory of beam bending analyzed in Ref. 3, we have

$$\frac{d^2z}{dx^2} = \frac{-\alpha_e}{J_y} \int T\, y\, d\, A \tag{5.5}$$

where

z is the transverse deflection of the beam,

α_e = coefficient of linear expansion

J_y = moment of inertia of the beam about the y axis

Eq. (5.5) is rewritten by evaluating the integral

$$\frac{d^2z}{dx^2} = -\alpha_e \frac{\Delta T}{t_c} = \text{a constant} \tag{5.6}$$

The expression for the thermal deflection is then given by

$$z = -\alpha_e \frac{\Delta T}{t_c} \frac{x^2}{2} \tag{5.7}$$

The thermal deflection can be mimimized by selecting a material of low coefficient of expansion or by using a material of high thermal conductivity. An increase in the thickness of the plate will also increase the temperature difference (Fig. 5.2) and also increase the weight of the plate. Hence, the parameter, t_c, should be as small as possible. The other important properties of materials not reflected in Eq. (5.7) are the density and the cost of the material as shown in Table 5.1.[4] For a beam of length 100m and thickness 0.01m, and made of polyamide (a low density and low cost material), the maximum thermal deflection is found to be approximately 7m.

If the beam is made of aluminum, the maximum deflection would be about 2mm. Once a tolerable thermal deflection is specified the material can be selected to meet the conflicting requirements of low density, high thermal conductivity, and low cost. In the next section the solar radiation pressure moment resulting from a thermally deflected beam (also applicable to a plate) is discussed.

V.4 Effect of Solar Radiation Pressure on a Thermally Deflected Beam (or Plate)

The moment expressions derived by Karymov (Eqns. 4.3-4.7) are used to obtain the moments acting on a thermally deflected beam. The equation for thermal deflection is given by (5.7). The moment on a completely absorbing surface is obtained (after integration) as,

$$\bar{N}_a = a_o\, c_o\, \delta_o\, \ell\, b\, \bar{j} \tag{5.8}$$

where

a_o, b_o, c_o are the direction cosines of the solar incident radiation vector

δ_o = maximum deflection (from Eq. (5.7)) = z_{max}

The maximum deflection, δ_o, can be obtained as a function of θ_i by selecting a function to represent ΔT in Fig. 5.2, and then by using the function for ΔT in Eq. (5.7). The moment acting on a completely reflecting surface is obtained through numerical integration, as,

$$\bar{N}_r = -0.05\, a_o\, c_o\, \delta_o\, \ell\, \bar{j} \tag{5.9}$$

The corresponding moment expressions for a plate are obtained as

$$\bar{N}_a = c_o\, \delta_o\, \ell\, b\, (b_o\bar{i} + a_o\bar{j})$$

$$\bar{N}_r = -0.05\, c_o\, \delta_o \ell b\, (b_o\bar{i} + a_o\ell\bar{j}) \tag{5.10}$$

The moment on a beam (or a plate) with a surface whose general coefficient of reflectivity is ε_r, can then be obtained by using Eq. (4.8).

References - Chapter V

1. Frisch, H.P., "Thermally Induced Response of Flexible Structures: A Method for Analysis," Journal of Guidance and Control, Vol. 3, No. 1, 1980, pp. 92-94.

2. Ayer, F. and Soosaar, K., "Structural Distortions of Space Systems due to Environmental Disturbances," AIAA International Meeting and Technical Display, "Global Technology 2000," May 6-8, 1980, Baltimore, Md., Paper No. AIAA - 80 - 0854.

3. Burgreen, D., Elements of Thermal Stress Analysis, C.P. Press, N.Y., 1971.

4. Ashton, J.E., Halpin, J.C. and Petit, P.H., Primer on Composite Materials Analysis, Technomic Publication, Conn., 197C.

Table 5.1. Properties of Representative Materials.[4]

Material	Density (Kg/m^3)	Expansion Coefficient, α_e ($m/m\ ^oC$)	Thermal Cond. K $KW/m-^oK$	≈ Cost ($/Kg)
Graphite	$1.5x10^3$	$8.3x10^{-5}$	$8.65x10^{-3}$	500
Beryllium	$1.8x10^3$	$3.5x10^{-6}$	$12.25x10^{-3}$	10,000
Aluminum	$2.7x10^3$	$2.1x10^{-6}$	$28.8x10^{-3}$	1.1
Polyamide	$1.13x10^3$	$25x10^{-6}$	$2.45x10^{-3}$	15

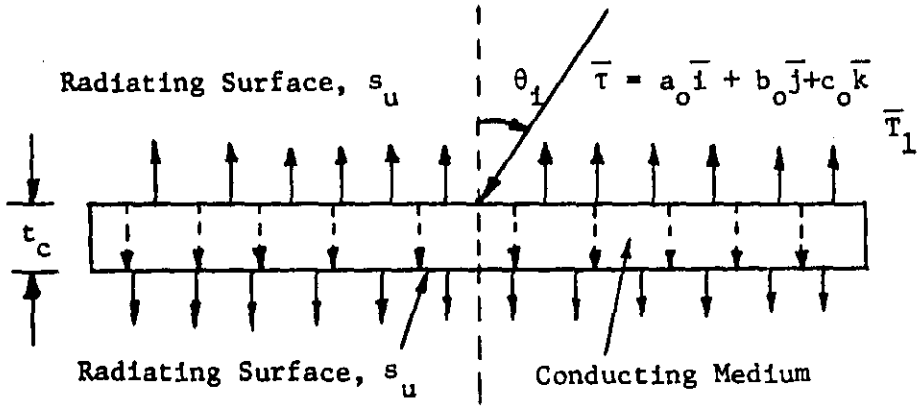

Fig. 5.1. Thermal Gradient in a Beam Due to Solar Radiation Heating.

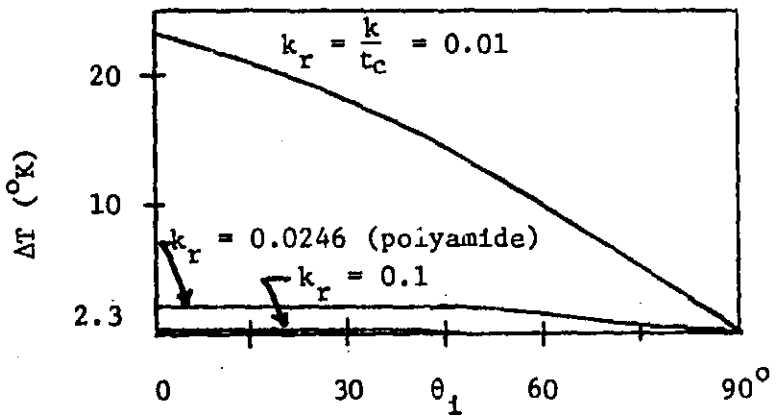

Fig. 5.2. Thermal Gradient in a Beam as a Function of Solar Incidence Angle and Thermal Conductivity.

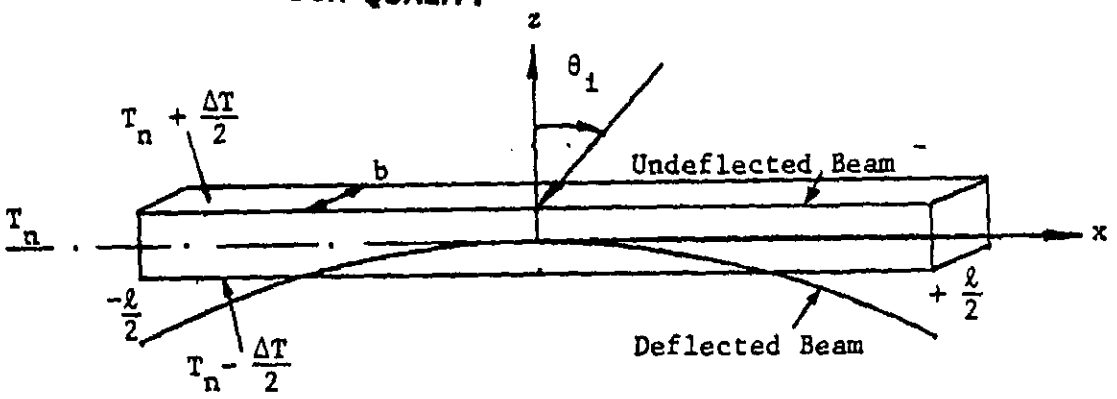

Fig. 5.3. Beam Bending Due to Solar Radiation Heating

VI. EVALUATION OF HOOP/COLUMN COUPLING COEFFICIENTS

The generic mode equations and the equations of rotational motion of a flexible orbiting body contain coupling terms between the rigid and flexible modes and terms due to the coupling within the flexible modes that are assumed to be small and, thus, are usually neglected when a finite element analysis of the dynamics of the system is undertaken. In this Chapter a computational algorithm that permits the evaluation of the coefficients in these coupling terms in the equations of motion as applied to a finite element model of the Hoop/Column system is developed.

Using a Newton-Euler approach, one-can express the equations of motion of an elemental mass of the system, in the frame moving with the body, as[1]

$$\{\bar{a}_{cm} + \ddot{\bar{r}} + 2\bar{\omega}\dot{\bar{r}} + \dot{\bar{\omega}}\bar{r} + \bar{\omega}\bar{\omega}\bar{r}\}\rho dv = \{\bar{f} + \bar{e} + L(\bar{q})/\rho\}\rho dv \qquad (6.1)$$

where ρ = mass per unit volume,

$\bar{e}$ = external forces per unit mass,

$\bar{q}$ = elastic transverse displacements of the element of volume.

$\bar{f}$ = force due to the gravity on the unit mass, and

L = the linear operator which when applied to $\bar{q}$ yields the elastic forces acting on the element of volume considered.

$\bar{r}$ = position vector of element dv

$\bar{\omega}$ = inertial angular velocity of the body frame

VI.1 EQUATIONS OF ROTATIONAL MOTION

The equations of rotational motion of the body are obtained by taking the moments of all the external, internal and inertial forces acting on the body, i.e., from Eq. (6.1)

$$\int \bar{r} \times [\bar{a}_{cm} + \ddot{\bar{r}} + 2\bar{\omega}\times\dot{\bar{r}} + \dot{\bar{\omega}}\times\bar{r} + \bar{\omega}\times(\bar{\omega}\times\bar{r})]\,\rho dv$$

$$= \int_v \bar{r}\times[L(\bar{q})/\rho + \bar{f} + \bar{e}]\,\rho dv \qquad (6.2)$$

one can obtain the following form for the equations of rotational motion.

$$\bar{R} + \sum_{n=1}^{\infty} \bar{Q}^{(n)} + \sum_{n=1}^{\infty} \bar{D}^{(n)} = \bar{G}_R + \sum_{n=1}^{\infty} \bar{G}^{(n)} + \bar{C} \qquad (6.3)$$

where $\bar{R} = \int_v [\bar{r}_o \times (\dot{\bar{\omega}}\times\bar{r}_o) - (\bar{r}_o\cdot\bar{\omega})\ (\bar{\omega}\times\bar{r}_o)]\ \rho dv$

$$\sum_{n=1}^{\infty} \bar{Q}^{(n)} = \int_v [\bar{r}_o\times\ddot{\bar{q}} + 2\bar{r}_o\times(\bar{\omega}\times\dot{\bar{q}}) + \dot{\bar{r}}_o\times(\bar{\omega}\times\bar{q}) + \bar{q}\times(\dot{\bar{\omega}}\times\bar{r}_o)$$
$$-(\bar{r}_o\cdot\bar{\omega})\ (\bar{\omega}\times\bar{q}) - (\bar{q}\cdot\bar{\omega})\ (\bar{\omega}\times\bar{r}_o)]\ \rho dv$$

$$\sum_{n=1}^{\infty} \bar{D}^{(n)} = \int_v \bar{q}\ \rho dv \times (\bar{a}_{cm} - \bar{f}_o) + \sum_{n=1}^{\infty} \omega_n^2 A_n \int_v \bar{r}_o \times \bar{\Phi}^{(n)}\ \rho dv$$

$$\bar{G}_R = \int \bar{r}_o \times M\bar{r}_o\ \rho dv$$

$$\sum_{n=1}^{\infty} \bar{G}^{(n)} = \int_v [\bar{r}_o \times M\bar{q} + \bar{q}\times M\bar{r}_o]\ \rho dv$$

$$\bar{C} = \int_v \bar{r}\times\bar{e}\ \rho dv$$

$\bar{r} = \bar{r}_o + \bar{q}$

M = matrix operator[1] which when applied to $\bar{r}$ yields gravity-gradient forces

$\bar{a}_{cm}$ = acceleration of the center of mass

$\bar{f}_o$ = force/mass due to gravity at the undeformed center of mass

$\bar{\Phi}^{(n)}$ = modal shape vector for the n^{th} mode

ω_n = frequency of the n^{th} mode

A_n = time dependent modal amplitude function

VI. 2 GENERIC MODE EQUATIONS

The generic mode equation is obtained by taking the modal components of all internal, external and inertial forces acting on the body, i.e.,

$$\int_v \bar{\Phi}^{(n)} \cdot [\bar{a}_{cm} + \ddot{\bar{r}} + 2\dot{\bar{\omega}}\bar{x}\dot{\bar{r}} + \dot{\bar{\omega}}\bar{x}\bar{r} + \bar{\omega}\bar{x}(\bar{\omega}\bar{x}\bar{r})]\, \rho dv$$

$$= \int_v \bar{\Phi}^{(n)} \cdot [L(\bar{q})/\rho + \bar{f} + \bar{e}]\, \rho dv \qquad (6.4)$$

The generic mode equation is obtained in the following form:

$$\ddot{A}_n + \omega_n^2 A_n + \varphi_n/M_n + \sum_{m=1}^{\infty} \varphi_{mn}/M_n = [g_n + \sum_{m=1}^{\infty} g_{mn} + E_n + D'_n]/M_n \qquad (6.5)$$

where $\varphi_n = \int_v [\bar{\Phi}^{(n)} \cdot \dot{\bar{\omega}}\bar{x}\bar{r}_o + \bar{\Phi}^{(n)} \cdot \bar{\omega}\bar{x}(\bar{\omega}\bar{x}\bar{r}_o)]\, \rho dv$

$$\sum_{m=1}^{\infty} \varphi_{mn} = \int_v [2\dot{\bar{\Phi}}^{(n)} \cdot \dot{\bar{\omega}}\bar{x}\dot{\bar{q}} + \bar{\Phi}^{(n)} \cdot \dot{\bar{\omega}}\bar{x}\bar{q} + \bar{\Phi}^{(n)} \cdot \bar{\omega}\bar{x}(\bar{\omega}\bar{x}\bar{q})]\, \rho dv$$

$$g_n = \int \bar{\Phi}^{(n)} \cdot \bar{M}\ddot{\bar{r}}_o \rho dv; \quad \sum_{m=1}^{\infty} g_{mn} = \int_v \bar{\Phi}^{(n)} \cdot \bar{M}\ddot{\bar{q}} \rho dv;$$

$$E_n = \int \bar{\Phi}^{(n)} \cdot \bar{e} \rho dv \text{ and } D'_n = \int_v \bar{\Phi}^{(n)} \rho dv \cdot (\ddot{\bar{a}}_{cm} - \bar{f}_o).$$

VI.3 CARTESIAN COMPONENTS OF THE DIFFERENT COUPLING TERMS

The expressions for $\bar{R}$, $\bar{Q}^{(n)}$, $\bar{G}_R$, $\bar{G}^{(n)}$, $\mathcal{Q}_n$, $\mathcal{Q}_{mn}$, g_n, g_{mn} in Cartesian components are presented in this section.

One can express the following vectors in their Cartesian component form as

$$\bar{r}_o = \xi_x \hat{i} + \xi_y \hat{j} + \xi_z \hat{k}; \quad \bar{\omega} = \omega_x \hat{i} + \omega_y \hat{j} + \omega_z \hat{k}$$

$$\bar{q} = \sum_{n=1}^{\infty} A_n(t) \bar{\phi}^{(n)}(\bar{r}_o); \quad \bar{\phi}^{(n)} = \phi_x^{(n)} \hat{i} + \phi_y^{(n)} \hat{j} + \phi_z^{(n)} \hat{k}$$

$$\bar{Q}^{(n)} = Q_x^{(n)} \hat{i} + Q_y^{(n)} \hat{j} + Q_z^{(n)} \hat{k}$$

and $$\bar{G}^{(n)} = G_x^{(n)} \hat{i} + G_y^{(n)} \hat{j} + G_z^{(n)} \hat{k},$$

where $\hat{i}$, $\hat{j}$, $\hat{k}$ are unit vectors along the body principal axes of inertia in the undeformed state; ξ_x, ξ_y, ξ_z are the coordinates of a point in the undeformed state.

With the use of the component forms of the vectors given above, one can expand the various vector expressions given in Eqs. (6.3) and (6.5) to obtain

$$\begin{aligned} \bar{R} = {} & [J_x \dot{\omega}_x + (J_z - J_y)\omega_y \omega_z] \hat{i} \\ & + [J_y \dot{\omega}_y + (J_x - J_z)\omega_z \omega_x] \hat{j} \\ & + [J_z \dot{\omega}_z + (J_y - J_x)\omega_x \omega_y] \hat{k} \end{aligned} \qquad (6.6)$$

$$Q_x^{(n)} = \ddot{A}_n(H_{yz}^{(n)}-H_{zy}^{(n)}) + 2\dot{A}_n[(H_{yy}^{(n)}+H_{zz}^{(n)})\omega_x - H_{yx}^{(n)}\omega_y - H_{zx}^{(n)}\omega_z] + A_n[2(H_{yy}^{(n)}+H_{zz}^{(n)})\dot{\omega}_x - (H_{xy}^{(n)}+H_{yx}^{(n)})\dot{\omega}_y - (H_{zx}^{(n)}+H_{xz}^{(n)})\dot{\omega}_z - 2\omega_y\omega_z(H_{zz}^{(n)}-H_{yy}^{(n)}) - \omega_x\omega_y(H_{xz}^{(n)}+H_{zx}^{(n)}) + \omega_x\omega_z(H_{xy}^{(n)}+H_{yx}^{(n)}) + (\omega_z^2-\omega_y^2)(H_{yz}^{(n)}+H_{zy}^{(n)})] \quad (6.7)$$

$$\bar{G}_R = (J_z-J_y)M_{23}\hat{i} + (J_x-J_z)M_{31}\hat{j} + (J_y-J_x)M_{21}\hat{k} \quad (6.8)$$

$$G_x^{(n)} = A_n[(M_{33}-M_{22})(H_{yz}^{(n)}+H_{zy}^{(n)}) - M_{21}(H_{xz}^{(n)}+H_{zx}^{(n)}) + M_{31}(H_{xy}^{(n)}+H_{yx}^{(n)}) + 2M_{23}(H_{yy}^{(n)}-H_{zz}^{(n)})] \quad (6.9)$$

$$\Phi_n = \dot{\omega}_x(H_{yz}^{(n)}-H_{zy}^{(n)}) + \dot{\omega}_y(H_{zx}^{(n)}-H_{xz}^{(n)}) + \dot{\omega}_z(H_{xy}^{(n)}-H_{yx}^{(n)}) + \omega_x\omega_y(H_{xy}^{(n)}+H_{yx}^{(n)}) + \omega_y\omega_z(H_{yz}^{(n)}+H_{zy}^{(n)}) + \omega_z\omega_x(H_{zx}^{(n)}+H_{xz}^{(n)}) - \omega_x^2(H_{yy}^{(n)}+H_{zz}^{(n)}) - \omega_y^2(H_{zz}^{(n)}+H_{xx}^{(n)}) - \omega_z^2(H_{xx}^{(n)}+H_{yy}^{(n)}) \quad (6.10)$$

$$\Phi_{mn} = 2\dot{A}_n[\omega_x(L_{yz}^{(mn)}-L_{zy}^{(mn)}) + \omega_y(L_{zx}^{(mn)}-L_{xz}^{(mn)}) + \omega_z(L_{xy}^{(mn)}-L_{yx}^{(mn)})] + A_m[\dot{\omega}_x(L_{yz}^{(mn)}-L_{zy}^{(mn)}) + \dot{\omega}_y(L_{zx}^{(mn)}-L_{xz}^{(mn)}) + \dot{\omega}_z(L_{xy}^{(mn)}-L_{yx}^{(mn)})$$

$$+ \omega_x\omega_y(L_{xy}^{(mn)}+L_{yx}^{(mn)}) + \omega_y\omega_z(L_{yz}^{(mn)}+L_{zy}^{(mn)})$$

$$+ \omega_z\omega_x(L_{zx}^{(mn)}+L_{xz}^{(mn)}) - \omega_x^2(L_{yy}^{(mn)}+L_{zz}^{(mn)})$$

$$- \omega_y^2(L_{zz}^{(mn)}+L_{xx}^{(mn)}) - \omega_z^2(L_{xx}^{(mn)}+L_{yy}^{(mn)})] \qquad (6.11)$$

$$g_n = \sum_{\alpha\beta}\sum H_{\alpha\beta}^{(n)} M_{\alpha\beta}$$

$$g_{mn} = A_m \sum_{\alpha\beta}\sum L_{\alpha\beta}^{(mn)} M_{\alpha\beta}$$

where $H_{\alpha\beta}^{(n)} = \int_v \xi_\alpha \phi_\beta^{(n)} dm$; $L_{\alpha\beta}^{(mn)} = \int_v \phi_\alpha^{(m)} \phi_\beta^{(n)} dm$; and $\alpha, \beta = x, y, z$ or $1, 2, 3$. When α is x in $H_{\alpha\beta}^{(n)}$ or $L_{\alpha\beta}^{(mn)}$ the corresponding value of α in $M_{\alpha\beta}$ is 1. In a similar way when α is y in $H_{\alpha\beta}^{(n)}$ or $L_{\alpha\beta}^{(mn)}$, α is 2 in $M_{\alpha\beta}$ and when α is z in $H_{\alpha\beta}^{(n)}$ or $L_{\alpha\beta}^{(mn)}$, α is 3 in $M_{\alpha\beta}$. The same reasoning holds for β also.

The expressions for $Q_y^{(n)}$ and $Q_z^{(n)}$ are obtained by the cyclic permutation of x, y, z in the expression for $Q_x^{(n)}$ in Eq. (6.7) and the expressions for $G_y^{(n)}$ and $G_z^{(n)}$ are obtained by the cyclic permutation of x, y, z in the expression for $G_x^{(n)}$ in Eq. (6.9).

For a discretized model the expressions for the volume integrals are replaced by the following summations:

$$H_{\alpha\beta}^{(n)} = \sum_{i=1}^{k} (\xi_\alpha)_i \, (\phi_\beta^{(n)})_i m_i \qquad (\alpha,\beta = x,y,z) \tag{6.12}$$

$$L_{\alpha\beta}^{(mn)} = \sum_{i=1}^{k} (\phi_\alpha^{(m)})_i \, (\phi_\beta^{(n)})_i m_i \tag{6.13}$$

where

k = total number of discrete masses

i = index identifying a nodal point

m_i = mass concentrated at the i^{th} node.

ξ_α = coordinates of m_i in the undeformed state

VI.4 EVALUATION OF COUPLING COEFFICIENTS IN THE EQUATIONS OF MOTION AS APPLIED TO A FINITE ELEMENT MODEL OF THE HOOP/COLUMN SYSTEM

VI. 4.1 Model Description

The structural dynamic modeling of the Hoop/Column antenna has gone through many stages before reaching the single surface model which will be analyzed in this chapter.

Initially, it had 231 nodes distributed as follows: 192 nodes on the 8 support circles including the hoop (24 nodes on each circle spaced at 15^{o} intervals); 28 nodes on the mast and the feed mast; and 11 nodes at the points of location of the solar panels (upper and lower), the S band reflector, and the feed panels (up-link and down-link)-see Figs. 5.1 and 5.2. After reduction the number of nodes was diminished to 114 including a total of 96 nodes on the circles: 1100, 1200, 1300, and 1400; 7 nodes on the mast and the feed mast; and 11 nodes at the locations of the solar panels, the S band reflector, and the feed panels (Fig. 6.1).

VI. 4.2 Approximate Mass Distribution

From an unpublished document prepared by the Harris Corporation,[2] and submitted by NASA Langley Research Center, it has been possible to arrive at the mass distribution shown in Table 6.1. 9803.0 lb. out of the total weight of the Hoop/Column Antenna (10,070 lb.) were distributed between the final grid points. The distribution was done in agreement with the information found in the Harris Corporation document. The page numbers appearing in Table 6.1 refer to particular mass/moment of inertia calculations in the Harris Corporation document.[2]

The small (2%) discrepancy between the calculated total mass (9803.0 lb.) and the stated weight of the system (10,070 lb) is thought to be attributed to: (1) uncertainties in the weight of specific stringers; (2) uncertainties inherent with the finite element reduction technique where the initial mass must be redistributed between a reduced, final number of grid (node) points; and (3) other miscellaneous uncertainties, such as the exact weight/location of the optical instrument, etc.

VI. 4.3 Cartesian Coordinates of all the Nodal Points in the Final NASTRAN Output

Reference 2 contains the cylindrical coordinates of all the nodal points on the mast, the feed mast, and at the location of the panels and electronics. It also contains the Z coordinates of the planes which contain the circles along with their respective diameters. Thus, the Cartesian coordinates of all the nodal points were obtained by a simple transformation from cylindrical to Cartesian coordinates.

VI.4.4 Development of a Computational Algorithm for Evaluation of the Coupling Coefficients

After receipt of the tape containing the modal functions, this information was stored in our IBM 360 in such a manner that when one calls subroutine, GETMP(2), he can refer to the k^{th} component of the I^{th} mode shape vector at the grid point J by VECMP(I,J,K). Based on this, an algorithm described in the flow diagram, Fig. 6.2, was designed and tested. As indicated in Fig. 6.2, the available data, such as: the Cartesian coordinates of the grid points on the mast, the feed mast and the ones at the locations on the appendages; and such as the mass concentrations at all the nodal points are input into the software routine and these data will consequently have to be updated according to any development in the Hoop/Column modeling. The subroutine, DCS, (given the radius of the circles and the Z component of their centers) computes the Cartesian coordinates of the nodal points on the circles.

Subroutine GETMP(2), which makes the $\phi_{J,k}^{(I)}$ available, is called and the values of components of the desired mode shape vector at the particular grid point are incorporated into a loop mathematically described by Eqs. (6.12) and (6.13). It should be noted that, for reasons of effectiveness, each coefficient is evaluated separately on the circles and on the other grid points and then combined to yield the corresponding coupling coefficient for the entire Hoop/Column system.

The algorithm has been tested for two modes (the 7^{th} and the 8^{th}) successfully, but only after the evaluation of the coefficients corresponding to all the 13 modes will one be able to make positive conclusions.

VI.4.5 Normalization of the Equations

In order to make a valid comparison between the terms in the rigid modes and the ones due to the coupling between the flexible modes, the equations of motion and the generic modal equations are non-dimensionalized in this section.

The Euler angles and their rates are assumed to have the following form:

$$\theta = \frac{\dot{\theta}_o}{\Omega} \sin \Omega t + \theta_o \cos \Omega t \text{ and } \dot{\theta} = \dot{\theta}_o \cos \Omega t - \theta_o \Omega \sin \Omega t$$

When $\theta_o \simeq 0$, the amplitude of θ is governed by that of $\dot{\theta}_o/\Omega$. In order to guarantee the small amplitude approximation for these angles, $\dot{\theta}/\Omega$ must have as a maximum the order of 1/10. For a gravity stabilized structure, Ω is proportional to the orbital angular velocity, ω_c, with the proportionality constant depending on the differences in appropriate moments of inertia, and whether pitch, roll, or yaw motion is under consideration. For this reason we select $\dot{\theta} \cong \omega_c/200\sqrt{3}$ and similarly for $\dot{\phi}_o$ and $\dot{\psi}_o$. (It is well known that the frequency of a rod shaped dumbbell librating near the local vertical is $\sqrt{3}\ \omega_c$). According to an assumed Euler sequence [(1)ϕ, (2)θ, and (3)ψ] from the local vertical to the principal body axes,

$$\omega_x = (\dot{\theta}-\omega_c)\sin \phi - \dot{\psi} \sin \theta \cos \phi$$

$$\omega_y = (\dot{\theta}-\omega_c)\cos \phi + \dot{\psi} \sin \theta \sin \phi$$

$$\omega_z = \dot{\psi} \cos \theta + \dot{\phi}$$

Therefore, $\omega_x \cong (\dot{\theta}-\omega_c)\phi - \dot{\psi}\theta \simeq 0$; $\omega_y \simeq (\dot{\theta}-\omega_c)$; and $\omega_z \cong \dot{\psi} + \dot{\phi}$ and the corresponding gravity gradient matrix operator, M^1, is calculated as

$$M = \omega_c^2 \begin{bmatrix} 2 & 0 & 0 \\ 0 & -1 & 0 \\ 0 & 0 & -1 \end{bmatrix}$$

The terms in the rigid modal equations are normalized by dividing each by $\ell^2\omega_7^2$ (where ℓ = 100m is selected as the characteristic length of the system and ω_7 is the frequency of the 7th mode); the terms in the generic modal equations are normalized by dividing by $\ell\omega_7^2$. The elastic displacements are assumed in such a manner that $\dot{A}_n \simeq \omega_n A_n$; $\ddot{A}_n \simeq \omega_n^2 A_n$. Examples of normalization follow:

$$G_x^{(n)}/\ell^2\omega_7^2 = A_n[(M_{33}-M_{22})(H_{yz}^{(n)}+ H_{zy}^{(n)}) - M_{21}(H_{xz}^{(n)}- H_{zx}^{(n)})$$

$$+ M_{31}(H_{xy}^{(n)} + H_{yx}^{(n)}) + 2M_{23}(H_{yy}^{(n)} - H_{zz}^{(n)})]/\ell^2\omega_7^2$$

$$\phi_n/\ell\omega_7^2 = \{\omega_7\omega_x(H_{yz}^{(n)} - H_{zy}^{(n)} + \omega_7\omega_y\ (H_{zx}^{(n)}- H_{xz}^{(n)}) + \omega_7\omega_z(H_{xy}^{(n)}- H_{yx}^{(n)})$$

$$+ \omega_x\omega_y(H_{xy}^{(n)} + H_{yx}^{(n)}) + \omega_y\omega_z\ (H_{yz}^{(n)} + H_{zy}^{(n)}) + \omega_z\omega_x\ (H_{zx}^{(n)}+ H_{xz}^{(n)})$$

$$- \omega_x^2\ (H_{yy}^{(n)} + H_{zz}^{(n)}) - \omega_y^2\ (H_{zz}^{(n)} + H_{xx}^{(n)}) - \omega_z^2\ (H_{xx}^{(n)} + H_{yy}^{(n)})\}/\ell\omega_7^2$$

In connection with the normalization of ϕ_n and similar terms involving time derivatives of the angular velocities, it should also be noted that $\frac{d}{dt} = \omega_7 \frac{d}{d\tau}$ where $\tau = \omega_7 t$, is a dimensionless time parameter.

VI.4.6 Comparison of the Terms

Table 6.2 shows the comparison between the magnitudes of the components of $\bar{R}$ and the components of the largest coupling coefficients in $\bar{Q}$ for both assumed values for A_n = 1m, 1mm for all modes.

It appears that when the system is operating within the mission specifications (deflections of the order of mm), the finite element assumptions are valid; when the deflections are of the order of meters the coupling between the flexible and rigid modes should be incorporated into the equations of motion.

In Table 6.3, a comparison of pertinent terms in the generic modal equations is given. $R_n = \ddot{A}_n + \omega_n^2 A_n$ is compared with $P_n = \{\phi_n - g_n + \sum_{m=7}^{13} (Q_{mn} - g_{mn})\}/M_n$ where M_n is the modal mass associated with the n^{th} mode. The comparison, after normalization of the different terms in the equations, shows that the time dependent amplitude of the modes can be approximated as an harmonic oscillator at least up to the point where A_n = 1m for all n.

One can therefore conclude that even though the time dependent modal amplitude function A_n can be modelled as an harmonic oscillator, the coupling between rigid and flexible modes has to be taken into consideration once the displacements exceed the order of mm, based on the parameters of the Hoop/Column system.

References - Chapter VI

1. Bainum, P.M., Kumar, V.K., and James, P.K., "The Dynamics and Control of Large Flexible Space Structures," NASA Report CR-156976, May 1978.

2. "Versatile Hoop/Column Antenna Structural Dynamic Model," unpublished document, Harris Corp, submitted by NASA Langley Research Center, (also including NASTRAN printout).

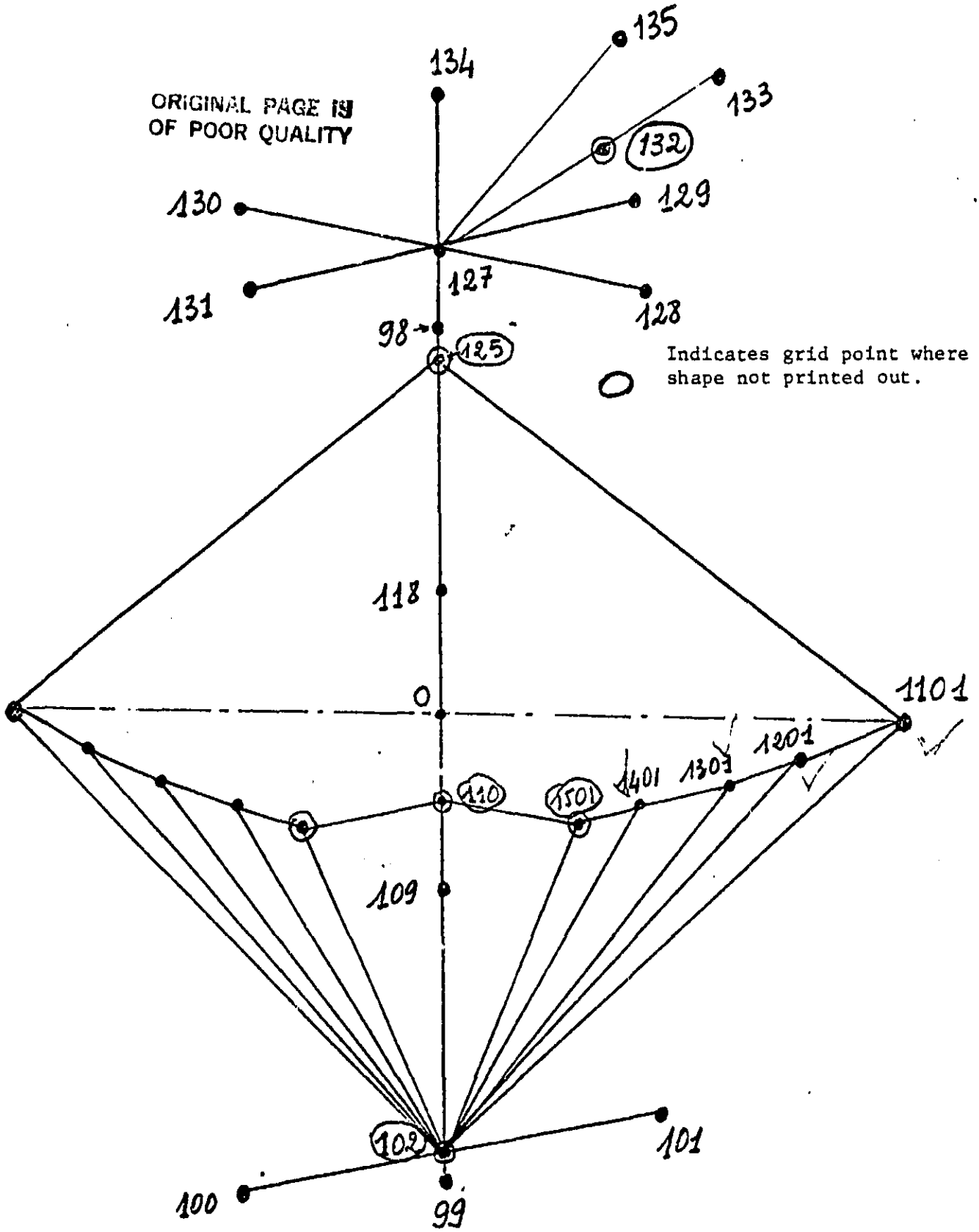

Fig. 6.1 Geometry of Single Surface Hoop/Column FEM Model.

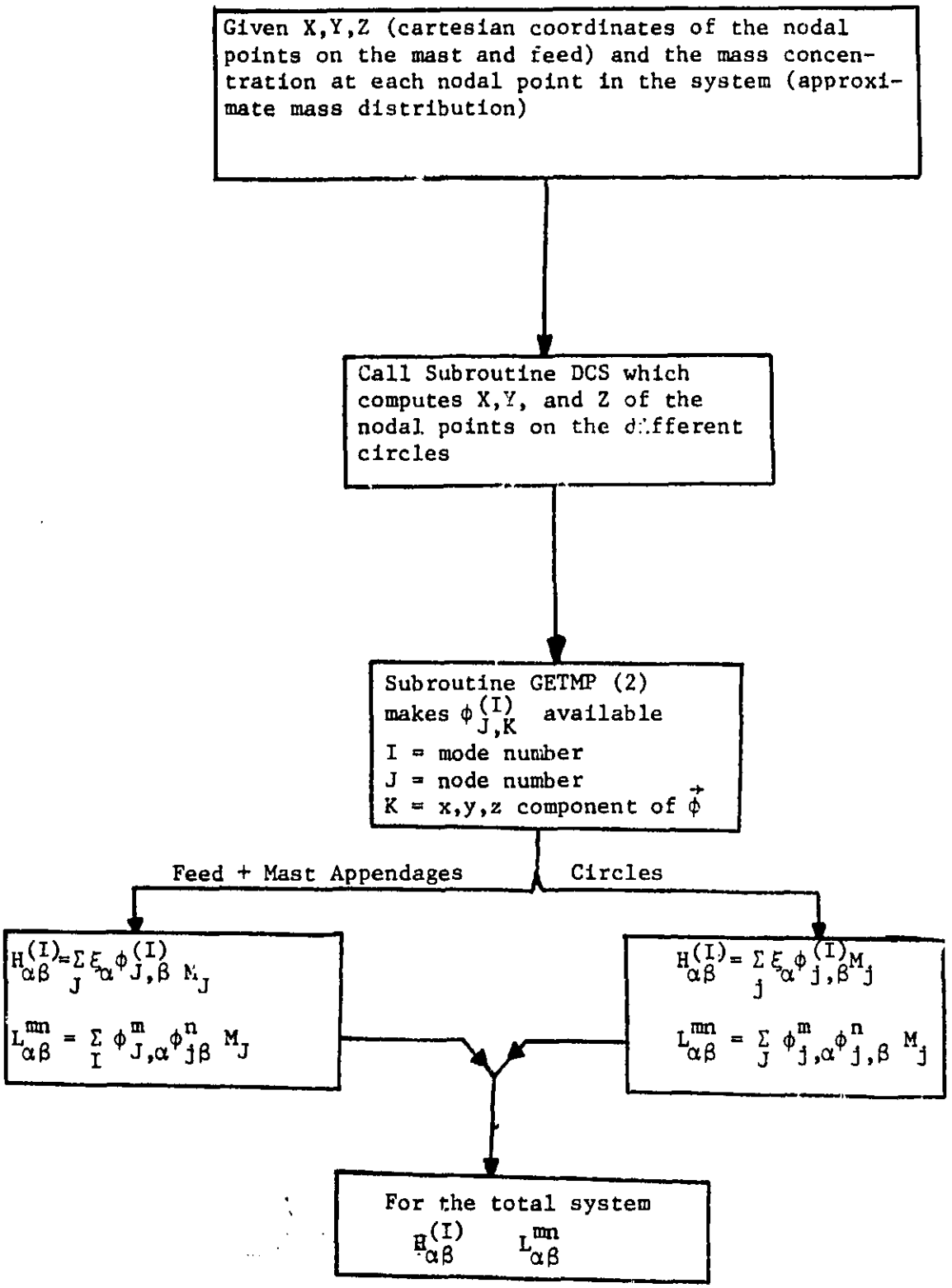

Fig. 6.2. Flow Diagram Describing the Algorithm Used in the Evaluation of the Coupling Coefficients.

Grid points I.D. No.	Mast Assemb.	Feed Mast Page 77	Lower Solar Panels Page 85	Upper Solar Panel Page 81	Feed Panels Page 82	S band Feed Page 86	S band Reflector Page 82	Lower Electronics Page 84	Upper Electronics Page 84	Hoop Assemb. + Mesh +Reflector	Sub. Total at grid points in lbs.
98	320.00	30.00									350.00
99	320.00							1953.00			2273.00
100			144.50								144.50
101			144.50								144.50
109	320.00										320.00
118	320.00										320.00
127		30.00		327.50					1898.00		2255.50
128					548.13						548.13
129					481.87						481.87
130					548.13						548.13
131					481.87						481.87
133						255.00					255.00
134							130.00				130.00
135				327.50							327.50
1100 series										1027.00	1027.00
1200 series										49.00	49.00
1300 series										49.00	49.00
1400 series										49.00	49.00
1500 series										49.00	49.00

** Hoop assembly at grid points 1101, 1107, 1113, 1119; 244.51bs/point

TOTAL 9803.0

Table 6.1 Approximate Mass Distribution at Final Grid Points (Pounds)

Table 6.2 Comparison of Pertinent Terms in the Rigid Modal Equations

A_n=1m

ection	R	$\sum_{n=7}^{13} Q_n$
X	1.48922 E-01	2.642388 E+00
Y	1.49854 E-01	-8.816196 E+00
Z	9.26317 E-02	-1.480150 E+00
A_n=1mm		
X	1.48922 E-01	2.642388 E-03
Y	1.49854 E-01	-8.816196 E-03
Z	9.26317 E-02	-1.480150 E-03

C-2

Table 6.3 Comparison of Pertinent Terms in the Generic Modal Equation

A = 1mm

Mode Number	Frequency rad/sec	Modal Mass	$R_n/\ell\omega_7^2$	$P_n/\ell\omega_7^2$
-	0.7489559	153.157	$.629344\times10^{-5}$	1.9543×10^{-8}
8	1.3692409	5.232954	$.210346\times10^{-4}$	-2.10287×10^{-10}
9	1.7471481	3.232954	$.34248\times10^{-4}$	8.7299×10^{-7}
10	3.2148494	0.3046446	$.115957\times10^{-3}$	-4.901252×10^{-5}
11	4.535031	1.992988	$.230747\times10^{-3}$	-3.46559×10^{-5}
12	5.5926659	723.5216	$.350924\times10^{-3}$	3.226×10^{-8}
13	5.7942225	0.6561203	$.376674\times10^{-3}$	4.678578×10^{-7}

A = 1m

Mode Number	Frequency rad/sec	Modal Mass	$R_n/\ell\omega_7^2$	$P_n/\ell\omega_7^2$
10	3.2148494	.3046446	.115957	$.4901252\times10^{-4}$
11	4.535031	1.992988	.230747	$.337854\times10^{-4}$
12	5.5926659	723.5216	.350924	3.2362×10^{-8}

VII. GENERAL CONCLUSIONS AND RECOMMENDATIONS

The graph theory approach has been utilized to define controllability in terms of term rank and input-state reachability concepts and applied to the placement of actuators for the proposed Hoop/Column system. The linear quadratic Gaussian techniques appear to offer greater flexibility to the controls designer in attempting to meet performance requirements while also maintaining propellant consumption at desired levels. System transient characteristics are noticeably degraded when an actuator, assumed to be mounted on the hoop, is then removed from the system. Before definitive conclusions can be arrived at relative to RMS pointing and surface accuracy requirements the effects of both sensor and plant noise and also environmental disturbances should be incorporated into the existing model and such studies have been initiated.

It is found that control laws previously designed for the case where environmental effects were neglected, may be inadequate to control the shape and orientation of very flexible beams that are exposed to solar radiation. For simple systems intuitive methods (suitable gain adjustments) of obtaining more robust closed-loop systems in the presence of the disturbances are indicated. For more complex flexible systems, such as platforms or antenna-type structures, numerical LQG techniques appear to offer the most promise and such studies are continuing.

Preliminary results evaluating the effect of thermally induced deflections due to solar heating of thin structures, indicate that

such deflections may give rise to appreciable disturbance torques, depending on the thermal properties and thickness of the materials used. Additional research in this important area is suggested.

A computer algorithm has been developed and used to evaluate the relative magnitude of coupling terms between the rigid rotational and flexible modes and also intra-modal coupling terms in the general equations of motion using the Hoop/Column mass and material properties. Such coupling terms are usually not included in finite element models based on the Earth-based vibrational and rigid modes only. It is seen that when the surface deflections are of the order of mm. (within mission specifications), that the relative magnitude of the largest of these coupling coefficients is at least one order of magnitude smaller than the principal coefficients. For surface deflections of the order of centimeters or even meters (still within the small amplitude deformation assumption) the coupling coefficients can be of the same order as the principal ones, indicating that these terms might have to be added to the finite element formulation if an accurate representation of the dynamics would be required.